J. Fluid Mech. (2004), *vol.* 510, *pp.* 303–331.
DOI: 10.1017/S0022112004009504 Printed in the United Kingdom

On the interaction of higher duct modes with a perforated liner system with bias flow

By JEFF D. ELDREDGE†

Department of Engineering, University of Cambridge, Trumpington Street, Cambridge CB2 1PZ, UK

(Received 10 July 2003 and in revised form 13 February 2004)

We explore the three-dimensional interaction of higher acoustic modes with bias-flow perforated liners in cylindrical and annular ducts. Pressure fluctuations in the vicinity of the liners excite the production and shedding of vorticity from the rims of apertures in the liners. An effective liner compliance is used which accounts for this transfer of acoustical into vortical energy. The investigation is facilitated by a Green's function solution of the Helmholtz equation in a lined section of duct, allowing calculation of the amplitudes of exiting wave modes due to incoming acoustic disturbances. A system containing an arbitrary number of concentric liners and the hollow cavities formed between them can be modelled. The results for an incident plane wave are compared with those from our previously developed one-dimensional model, with excellent agreement. We demonstrate that results for all modes that travel parallel to the liner, including higher circumferential modes in narrow annular gaps, exhibit self-similar behaviour, and that liner design rules developed for planar duct modes can be adapted accordingly. The acoustic absorption can be strongly enhanced by downstream duct reflection for wavelengths larger than twice the liner length, but is less affected at higher frequencies that allow persistent pressure minima along the liner. Across larger frequency ranges, the liner systems are shown to permit two types of resonance associated with the duct and the cavities, respectively, and a third of Helmholtz type, associated with the system as a whole. The effect of these resonances on incident modes is demonstrated, and, in particular, we explore their enhancement of acoustic absorption.

1. Introduction

Engineering systems such as industrial gas turbines are often operated in conditions that make them susceptible to acoustically driven combustion instabilities. The large pressure fluctuations associated with these instabilities can degrade the performance of the device and potentially cause structural damage, and passive damping techniques are frequently used to attempt to mitigate their growth. For cooling purposes, perforated liner systems which introduce steady flow through regular arrays of circular apertures are often incorporated into the walls of a combustion chamber. The cooled walls may consist of multiple layers of liners for a more effective distribution of cool air. In addition, the steady bias flow can also enhance the acoustic absorption by the liner, and thus such a system can effectively serve both purposes. In previous work (Eldredge & Dowling 2003), we investigated the absorptive properties of the liner

† Present address: Mechanical & Aerospace Engineering Department, University of California, Los Angeles 90095-1597, USA.

system when only planar duct modes are present. Acoustically driven instabilities may also contain higher modes, however, and in this paper we seek to characterize the response of such liner systems to general acoustic modes in cylindrical and annular ducts.

The physical mechanism responsible for acoustic absorption in a bias-flow liner is the generation of fluctuating vorticity at the rim of each aperture, creating a dipole-like sink which removes energy from the nearby sound field. The vorticity is subsequently convected away by the mean jet and dissipated into heat. This mechanism for the transformation of acoustic energy into vortical energy occurs in many geometries (e.g. Bechert 1980; Howe 1980), and has been reviewed by Crighton (1981). Howe (1979) determined the unsteady flow in an aperture through which a steady high-Reynolds-number flow passes by solving the Poisson equation for the fluctuating stagnation enthalpy and using an unsteady Kutta condition to determine the amount of vorticity produced. By virtue of the mean flow, the fluctuating sound field and resultant vorticity are linearly related. Hence the Rayleigh conductivity for the aperture, which quantifies the ratio of its unsteady volume flux to the pressure difference across it, is independent of the amplitude of the sound field. Provided the vorticity does not interact with another receptive edge, no sound is produced by this process – the sound produced by the quadrupole sources in the jet issuing from the aperture is uniformly weaker at all Strouhal numbers.

In the absence of a mean flow, vorticity can still be produced unsteadily at the aperture rim if the incident sound field is sufficiently large. Under such conditions, the Rayleigh conductivity contains a term that is proportional to the acoustic velocity. This nonlinear mechanism has been explored by Cummings & Eversman (1983) in the context of duct terminations and by Cummings (1983) for orifice plates.

The problem of wave propagation in ducts with acoustically lined walls is classical (see e.g. Morse & Ingard 1968). Ducts that are comprised of wall segments of different acoustic properties were considered by Lansing & Zorumski (1973), who explored the reflection and transmission from a discontinuity of wall impedance by matching pressure and velocity across the discontinuity. They evaluated their procedure by comparing with a Wiener–Hopf solution for the case of a two-dimensional duct with an impedance change on only a single wall, and found that the inclusion of only a few cutoff modes was required for agreement.

Screens and liners of the type considered here, with steady flows issuing through regular arrays of apertures, have been previously explored, as well. Howe (1979) extended his single-aperture result to examine the reflection and transmission properties of a screen subjected to an incident plane wave. Provided the apertures are sufficiently far apart, the vorticity shed by one aperture has no effect on the flow through another, and thus the apertures contribute independently to the acoustic characteristics of the screen. When the screen is backed by a cavity and rigid wall, absorption is enhanced by the additional interaction of the energy reflected by the wall. An infinite backed screen was investigated both theoretically and experimentally by Hughes & Dowling (1990), who found that absorption was largest at frequencies that they identified with a Helmholtz-type resonance of the volume behind each aperture. With an interest in exploring transverse-type duct resonances, they extended their analysis to examine the altered properties of an infinitely long cylindrical duct when the wall is lined with such a backed screen. Though these liners are effective as passive devices, active control techniques may be used to increase their range of utility. Zhao & Sun (1999) explored the active tuning of both the cavity depth and bias flow of a liner to achieve either maximum absorption or specified wall impedance.

These analyses all assumed the liner to be infinitesimally thin, but the finite thickness of a real liner increases its reactance owing to the inertia of fluid in each aperture, as was confirmed experimentally by Jing & Sun (1999). Further 'real flow' effects – such as viscous effects in the aperture flow and reactance of the external flow – were incorporated into the impedance model developed by Bellucci, Paschereit & Flohr (2002).

In previous work (Eldredge & Dowling 2003), we developed a one-dimensional model for planar duct modes interacting with a finite-length system consisting of multiple layers of bias-flow perforated liners. An effective wall compliance was used for each liner, based on the aperture Rayleigh conductivity developed by Howe (1979). When compared with the results from our experimental investigation, we found excellent agreement for a wide range of frequencies and bias flows. The model was used to develop a set of design rules for such liner systems.

In this work, we extend the results of Eldredge & Dowling (2003) to higher duct modes. Our approach will again be to model the liners with effective compliances, and employ a Green's function to solve for the fluctuating pressure distribution in the lined section of duct. The Green's function will decouple the duct from the surrounding cavities, and the resulting integral equation will only involve the normal derivative of the pressure on the interfaces with the adjacent rigid-walled sections. By matching pressure and velocity across the duct interfaces and projecting onto the duct eigenfunctions, the integral equation is subsequently reduced to a system of equations for the unknown modal amplitudes in terms of the prescribed incident mode.

In § 2, we develop the Green's function solution approach for an arbitrary system of liners and cavities. We also develop an expression for the acoustic absorption of the system, which will be used as a metric for characterizing the behaviour of the system in § 3. In this section we will examine the response of different liner systems to planar, circumferential and radial modes. The first two we categorize as 'grazing modes' because of their tendency to travel parallel to the walls of the duct, and their interactions with the liner are shown to reduce to a self-similar form. Across larger frequency ranges, we identify three classes of resonances associated with the duct, the cavities and the Helmholtz resonance of the overall liner system, respectively. We also present an approach for maximizing the broadband absorption at high frequencies through adjustment of the aperture flow to shift the peak liner resistance. Finally, conclusions are drawn in § 4. In the Appendix, further details are provided for the development of the solution approach presented in § 2.

2. Model development

The goal of the model is to predict the acoustic scattering of an incoming disturbance by a system consisting of an arbitrary number of concentric liners. We do so by developing an equation in which the pressure fluctuations in a lined section of duct are expressed solely in terms of surface integrals over the duct cross-section upstream and downstream of the liner. Such an expression can then be transformed into a scattering matrix for the incident disturbance amplitudes.

Consider an axisymmetric geometry as shown in figure 1. Two annular sections of duct, with rigid inner and outer walls of radii r_0 and r_1, respectively, are joined by a section of axial length L. This intermediate section also has a rigid inner wall of radius r_0, but its outer wall is replaced by a cylindrical liner of radius r_1, uniform compliance η_1 and small thickness $t_1 \ll r_1 - r_0$. This liner is surrounded (radially) by an arbitrary number N_l of cylindrical liners of the same axial length and with radii

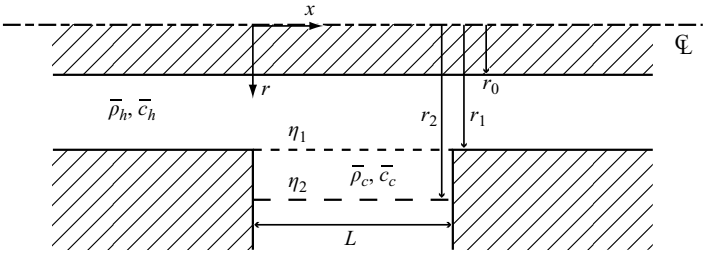

FIGURE 1. Configuration of lined section of annular duct.

$r_2, r_3, \ldots, r_{N_l}$, uniform compliances $\eta_2, \eta_3, \ldots, \eta_{N_l}$, and small thicknesses $t_2, t_3, \ldots, t_{N_l}$. Adjacent liners form a hollow cavity between them, closed at each axial end by a rigid wall. The sequence of liners may be truncated by either a plenum (in lieu of the outermost cavity) or a rigid wall (in lieu of the outermost liner). Thus, the simplest configuration – beyond the trivial case of an unlined duct – would consist of a single liner surrounded by a plenum. The mean density and speed of sound in the duct are $\bar{\rho}_h$ and $\bar{c}_h$, and are $\bar{\rho}_c$ and $\bar{c}_c$ in the liner cavities. We will use the term 'upstream' to denote the section of duct in which the source of the incident acoustic wave lies, and 'downstream' to describe the duct on the other side of the lined section.

2.1. *Governing equations*

Suppose that a small perturbation to the pressure is in the form

$$p_m(r, x)\mathrm{e}^{\mathrm{i}(\omega t - m\phi)}.$$

We are permitted to consider circumferential modes independently, owing to the axisymmetry of the geometry and the linearity of the problem. The amplitude of this perturbation is governed by a modified Helmholtz equation. In the duct, this is expressed in cylindrical coordinates as

$$\frac{1}{r}\frac{\partial}{\partial r}\left(r\frac{\partial p_m}{\partial r}\right) + \frac{\partial^2 p_m}{\partial x^2} + \left(k_h^2 - \frac{m^2}{r^2}\right) p_m = 0, \tag{2.1}$$

where $k_h \equiv \omega/\bar{c}_h$. The axial coordinate, x, is measured from the left-hand end of the lined section. Note that no mean duct flow is included in this analysis. The small duct flow that grows from the contribution of the liner bias flow is assumed to be of sufficiently small Mach number that its effect is negligibly small. In the liner cavities, the governing equation is

$$\frac{1}{r}\frac{\partial}{\partial r}\left(r\frac{\partial p_m}{\partial r}\right) + \frac{\partial^2 p_m}{\partial x^2} + \left(k_c^2 - \frac{m^2}{r^2}\right) p_m = 0, \tag{2.2}$$

where $k_c \equiv \omega/\bar{c}_c$.

We now partition an (r, x)-slice of the lined section into subdomains, as depicted in figure 2. The first domain, Ω_0, resides in the duct and is bounded by the inner wall of the annulus, the interfaces with the rigid-walled sections upstream and downstream, and the inward side of the first liner. The other domains are contained by the liner cavities. For example, domain Ω_1 is bounded by the outward side of the first liner, the rigid transverse barriers, and the inward side of the second liner. For modelling purposes, it is adequate to regard each liner as infinitesimally thin, and the domain boundaries that are adjacent to it as common. The physical thickness of the liner can be incorporated into its compliance, as demonstrated in § 2.4.

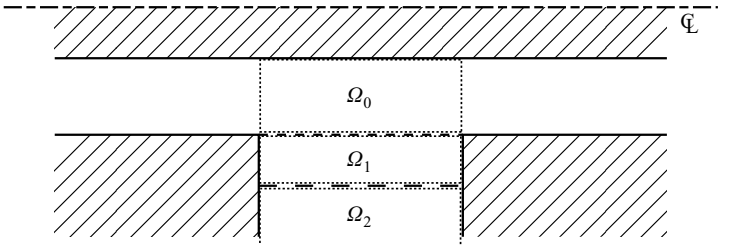

FIGURE 2. Partition of lined section into subdomains.

The rigid-walled boundaries impose no-through-flow conditions on the velocity, and thus vanishing normal derivative of the pressure. For the conditions at the liners, we recall the definition of the compliance given by Leppington (1977), as the ratio of the normal derivative of the pressure fluctuation p_m at a compliant wall to the jump in p_m across the wall. Thus, conditions of this sort will be of the form

$$\frac{\partial p_m}{\partial n} = \eta \, [p_m]_{0^-}^{0^+} . \tag{2.3}$$

We hypothesize a thin layer of fluid adjacent to the inward side of the first liner, in which the mean conditions are identical to those in the liner cavities, $\bar{\rho}_c$ and $\bar{c}_c$. Across the interface of this layer with the rest of the duct, the pressure and normal velocity are continuous (strictly, the particle displacement is continuous, but, with a lack of mean axial flow, this is equivalent to continuous normal velocity). Thus, for a system of N_l liners, we have

$$\frac{\partial p_m}{\partial r}(r_0, x) = 0, \tag{2.4a}$$

$$\frac{\partial p_m}{\partial r}(r_1^-, x) = \eta_1 \frac{\bar{\rho}_h}{\bar{\rho}_c}[p_m(r_1^+, x) - p_m(r_1^-, x)], \tag{2.4b}$$

$$\frac{\partial p_m}{\partial r}(r_1^+, x) = \frac{\bar{\rho}_c}{\bar{\rho}_h}\frac{\partial p_m}{\partial r}(r_1^-, x), \tag{2.4c}$$

$$\frac{\partial p_m}{\partial r}(r_k^-, x) = \eta_k[p_m(r_k^+, x) - p_m(r_k^-, x)], \tag{2.4d}$$

$$\frac{\partial p_m}{\partial r}(r_k^+, x) = \frac{\partial p_m}{\partial r}(r_k^-, x), \tag{2.4e}$$

for $x \in [0, L]$, and by virtue of the rigid cavity walls at $x = 0$ and $x = L$,

$$\frac{\partial p_m}{\partial x}(r, 0) = \frac{\partial p_m}{\partial x}(r, L) = 0, \tag{2.4f}$$

for $r \in [r_{k-1}, r_k]$ and $k = 2, 3, \ldots, N_l$. The series of conditions is concluded by either a plenum external to the outermost liner, for which the final condition would be

$$\frac{\partial p_m}{\partial r}\left(r_{N_l}^-, x\right) = -\eta_{N_l} p_m\left(r_{N_l}^-, x\right), \quad x \in [0, L], \tag{2.5}$$

or a rigid wall replacing the outermost liner at r_{N_l}, for which the condition is simply

$$\frac{\partial p_m}{\partial r}\left(r_{N_l}^-, x\right) = 0, \quad x \in [0, L]. \tag{2.6}$$

It is also necessary to constrain the acoustic energy density to be integrable as the interfaces $x = 0, L$ are approached along the lined wall, i.e. at $r = r_1^-$ and $x = 0^+$ and

$x = L^-$. This condition ensures that no energy is created at the discontinuity in wall compliances. To satisfy these constraints, it is sufficient to require that the solution and its first spatial derivatives are bounded at these points.

The conditions at the interfaces $x = 0$ and $x = L$, $r \in [r_0, r_1]$, are derived from enforcing continuity of pressure and velocity across these boundaries. However, the fluctuating conditions immediately upstream of $x = 0$ and downstream of $x = L$ are not entirely known, and in fact represent the quantities we hope to solve for. We can write the pressure in the upstream section in terms of eigenfunctions as

$$p_m(r, x) = \sum_q (\alpha_q^+ \exp(-\mathrm{i}\kappa_q x) + \alpha_q^- \exp(\mathrm{i}\kappa_q x)) \Gamma_m(\gamma_q r_0, \gamma_q r), \quad x < 0. \tag{2.7}$$

In terms of the Bessel functions of the first and second kind, J_m and Y_m respectively, the radial eigenfunction for an annular duct is

$$\Gamma_m(a, b) \equiv Y_m'(a) J_m(b) - J_m'(a) Y_m(b), \tag{2.8}$$

or simply

$$\Gamma_m(a, b) \equiv J_m(b) \tag{2.9}$$

for a cylindrical one. The rigid duct walls restrict the set of radial wavenumbers, γ_q, $q = 0, 1, \ldots, \infty$, to the roots of the equation $\Gamma_m'(\gamma r_0, \gamma r_1) = 0$, where

$$\Gamma_m'(a, b) \equiv \frac{\partial}{\partial b} \Gamma_m(a, b) = \begin{cases} Y_m'(a) J_m'(b) - J_m'(a) Y_m'(b) & \text{(ann.)}, \\ J_m'(b) & \text{(cyl.)}. \end{cases} \tag{2.10}$$

The axial wavenumbers are related to these by

$$\kappa_q = \begin{cases} \left| k_h^2 - \gamma_q^2 \right|^{1/2}, & k_h > \gamma_q, \\ -\mathrm{i} \left| \gamma_q^2 - k_h^2 \right|^{1/2}, & k_h < \gamma_q. \end{cases} \tag{2.11}$$

The axial derivative of the pressure in $x < 0$ is given by

$$\frac{\partial p_m}{\partial x}(r, x) = -\mathrm{i} \sum_q \kappa_q (\alpha_q^+ \exp(-\mathrm{i}\kappa_q x) - \alpha_q^- \exp(\mathrm{i}\kappa_q x)) \Gamma_m(\gamma_q r_0, \gamma_q r). \tag{2.12}$$

Similarly, in the downstream section, $x > L$, the solutions are

$$p_m(r, x) = \sum_q (\beta_q^+ \exp(-\mathrm{i}\kappa_q (x - L)) + \beta_q^- \exp(\mathrm{i}\kappa_q (x - L))) \Gamma_m(\gamma_q r_0, \gamma_q r), \tag{2.13}$$

$$\frac{\partial p_m}{\partial x}(r, x) = -\mathrm{i} \sum_q \kappa_q (\beta_q^+ \exp(-\mathrm{i}\kappa_q (x - L)) - \beta_q^- \exp(\mathrm{i}\kappa_q (x - L))) \Gamma_m(\gamma_q r_0, \gamma_q r). \tag{2.14}$$

The axial waveform in this section has been referenced to $x = L$, which ensures a more accurate numerical solution for the amplitudes of modes that are evanescent at the downstream interface.

Ultimately, we will suppose that the incident amplitudes, α_q^+, are known, and that β_q^- are related to β_q^+ through a reflection from the downstream configuration. For now, however, we will leave these pressures in their present form and proceed to the solution approach.

2.2. *Solution scheme*

In the Appendix, a decoupled integral equation is developed for the pressure, which we quote here

$$p_m(r,x)=\int_{r_0}^{r_1} r'\tilde{G}_m(r,x|r',0)\frac{\partial p_m}{\partial x}(r',0)\,\mathrm{d}r'-\int_{r_0}^{r_1} r'\tilde{G}_m(r,x|r',L)\frac{\partial p_m}{\partial x}(r',L)\,\mathrm{d}r'. \quad (2.15)$$

This equation has the advantage of only involving surface integrals over the duct cross-section upstream and downstream of the lined section; the effects of liners and their neighbouring cavities are contained entirely in the decoupling Green's function, $\tilde{G}_m$. Equation (2.15) serves as the basis for the solution scheme to compute the scattering of an incident acoustic wave by the liner system. When we evaluate the equation on the cross-section boundaries at $x=0$ and $x=L$, match the pressures across them, and then project the equation onto the space of rigid-walled eigenfunctions, we are left with an infinite system of equations for the unknown reflection and transmission amplitudes. This system can be judiciously truncated to form a numerical scheme.

First, we substitute expressions (2.12) and (2.14) for the respective pressure derivatives in the surface integrals of (2.15). We use the decoupling Green's function in its cosine expansion form, as given by (A 22). The resulting expression for the pressure can be written as

$$\begin{aligned}p_m(r,x)=&-\mathrm{i}\sum_q\frac{\kappa_q}{L}(\alpha_q^+-\alpha_q^-)\sum_{n=-\infty}^{\infty}\cos\left(\frac{n\pi x}{L}\right)\int_{r_0}^{r_1} r'\tilde{R}_n(r,r')\Gamma_m(\gamma_q r_0,\gamma_q r')\,\mathrm{d}r'\\&+\mathrm{i}\sum_q\frac{\kappa_q}{L}(\beta_q^+-\beta_q^-)\sum_{n=-\infty}^{\infty}(-1)^n\cos\left(\frac{n\pi x}{L}\right)\int_{r_0}^{r_1} r'\tilde{R}_n(r,r')\Gamma_m(\gamma_q r_0,\gamma_q r')\,\mathrm{d}r'.\end{aligned} \quad (2.16)$$

The integral that appears in both terms can be evaluated analytically, and after some manipulation we arrive at

$$\begin{aligned}p_m(r,x)=&-\mathrm{i}\sum_q(\alpha_q^+-\alpha_q^-)\Gamma_m(\gamma_q r_0,\gamma_q r)\frac{\kappa_q}{L}\sum_n\frac{\cos(n\pi x/L)}{\tilde{\gamma}_n^2-\gamma_q^2}\\&+\mathrm{i}\sum_q(\beta_q^+-\beta_q^-)\Gamma_m(\gamma_q r_0,\gamma_q r)\frac{\kappa_q}{L}\sum_n\frac{(-1)^n\cos(n\pi x/L)}{\tilde{\gamma}_n^2-\gamma_q^2}\\&-\mathrm{i}\sum_q(\alpha_q^+-\alpha_q^-)\tilde{C}_q^s(r,x)+\mathrm{i}\sum_q(\beta_q^+-\beta_q^-)\tilde{C}_q^c(r,x),\end{aligned} \quad (2.17)$$

where the coupling functions are defined as

$$\tilde{C}_q^s(r,x)=\eta_1\frac{\bar{\rho}_h}{\bar{\rho}_c}\Gamma_m(\gamma_q r_0,\gamma_q r_1)\frac{\kappa_q}{L}\sum_n\frac{D^{(0)}_{n,<}(\tilde{\gamma}_n r_0,\tilde{\gamma}_n r)}{\tilde{\gamma}_n D^{(0)'}_{n,<}(\tilde{\gamma}_n r_0,\tilde{\gamma}_n r_1)}\frac{\Lambda_n}{\tilde{\gamma}_n^2-\gamma_q^2}\cos\left(\frac{n\pi x}{L}\right), \quad (2.18)$$

$$\tilde{C}_q^c(r,x)=\eta_1\frac{\bar{\rho}_h}{\bar{\rho}_c}\Gamma_m(\gamma_q r_0,\gamma_q r_1)\frac{\kappa_q}{L}\sum_n\frac{D^{(0)}_{n,<}(\tilde{\gamma}_n r_0,\tilde{\gamma}_n r)}{\tilde{\gamma}_n D^{(0)'}_{n,<}(\tilde{\gamma}_n r_0,\tilde{\gamma}_n r_1)}\frac{(-1)^n\Lambda_n}{\tilde{\gamma}_n^2-\gamma_q^2}\cos\left(\frac{n\pi x}{L}\right). \quad (2.19)$$

At first glance, it does not appear that (2.17) will satisfy the condition of continuous axial velocity (or equivalently, axial pressure derivative) at the interfaces $x=0$ and $x=L$, due to the expansion in cosines. However, the cosine series in the first two

terms converge uniformly to analytical expressions:

$$\frac{\kappa_q}{L}\sum_{n=-\infty}^{\infty}\frac{\cos(n\pi x/L)}{\tilde{\gamma}_n^2-\gamma_q^2}=\kappa_q L\sum_{n=-\infty}^{\infty}\frac{\cos(n\pi x/L)}{\kappa_q^2L^2-n^2\pi^2}=\frac{\cos\kappa_q(x-L)}{\sin\kappa_q L},\tag{2.20}$$

$$\frac{\kappa_q}{L}\sum_{n=-\infty}^{\infty}\frac{(-1)^n\cos(n\pi x/L)}{\tilde{\gamma}_n^2-\gamma_q^2}=\kappa_q L\sum_{n=-\infty}^{\infty}\frac{(-1)^n\cos(n\pi x/L)}{\kappa_q^2L^2-n^2\pi^2}=\frac{\cos\kappa_q x}{\sin\kappa_q L},\tag{2.21}$$

and thus the pressure in the lined section of duct can be written as

$$\begin{aligned}p_m(r,x)=&-\mathrm{i}\sum_q\left[(\alpha_q^+-\alpha_q^-)\frac{\cos\kappa_q(x-L)}{\sin\kappa_q L}-(\beta_q^+-\beta_q^-)\frac{\cos\kappa_q x}{\sin\kappa_q L}\right]\Gamma_m(\gamma_q r_0,\gamma_q r)\\&-\mathrm{i}\sum_q(\alpha_q^+-\alpha_q^-)\tilde{C}_q^s(r,x)+\mathrm{i}\sum_q(\beta_q^+-\beta_q^-)\tilde{C}_q^c(r,x).\end{aligned}\tag{2.22}$$

Mathematically, the terms in square brackets represent a smooth transition between the boundary values of the axial velocity at $x=0$ and $x=L$; upon differentiation with respect to x, one of these terms vanishes at either interface. If instead the terms inside the series (2.20) and (2.21) had been differentiated directly, the resulting sine series would not converge uniformly to the derivatives of the expressions on the right-hand side. Also, it is important to note that the remaining two coupling terms in (2.22) have vanishing axial derivatives at the boundaries $x=0, L$, for they represent the direct effect of the cavity pressures, which themselves have vanishing derivatives. Thus, the infinite series in these terms are themselves uniformly convergent. It can be easily verified by differentiating (2.22) with respect to x and comparing with (2.12) and (2.14) at $x=0$ and $x=L$, respectively, that the condition of continuous axial velocity at the interfaces is indeed satisfied.

A physical interpretation of (2.22) is also readily available. As acoustic waves travel from either upstream or downstream into the lined section, they are continuously partitioned into a transmitted part and a reflected part at every axial position owing to the presence of the liner. The propagation of the waves is controlled by the first term of (2.22), while the final two terms in (2.22) represent the machinery for effecting the partition, through excitation of a liner velocity flux, which requires the combined contribution from all travelling modes. In the simple case of a rigid duct, the coupling terms vanish, and the first term reduces to two uncoupled non-decaying travelling waves.

The solution procedure is developed through a straightforward matching of pressure at the interfaces. We alternately set the pressure expression (2.22) at $x=0$ equal to the upstream duct pressure there, given by (2.7), and at $x=L$ to the downstream duct pressure, given by (2.13). Both sides of these equations are multiplied by $r\Gamma_m(\gamma_p r_0,\gamma_p r)$, with arbitrary p, and integrated over $r\in[r_0,r_1]$. The duct cross-section eigenfunctions are orthogonal, and thus the resulting infinite systems of algebraic equations are

$$\begin{aligned}\alpha_p^+-\alpha_p^-=&-\mathrm{i}(\alpha_p^+-\alpha_p^-)\cot\kappa_p L+\mathrm{i}(\beta_p^+-\beta_p^-)\csc\kappa_p L\\&-\mathrm{i}\sum_q C_{pq}^s(\alpha_q^+-\alpha_q^-)+\mathrm{i}\sum_q C_{pq}^c(\beta_q^+-\beta_q^-),\end{aligned}\tag{2.23}$$

$$\begin{aligned}\beta_p^++\beta_p^-=&-\mathrm{i}(\alpha_p^+-\alpha_p^-)\csc\kappa_p L+\mathrm{i}(\beta_p^+-\beta_p^-)\cot\kappa_p L\\&-\mathrm{i}\sum_q C_{pq}^c(\alpha_q^+-\alpha_q^-)+\mathrm{i}\sum_q C_{pq}^s(\beta_q^+-\beta_q^-),\end{aligned}\tag{2.24}$$

for all $p \in [0, \infty)$, where the modal coupling matrices, C^s_{pq} and C^c_{pq}, are defined as

$$C^{s,c}_{pq} \equiv \frac{1}{\|\Gamma_{m,p}\|^2} \int_{r_0}^{r_1} r \tilde{C}^{s,c}_q(r, 0) \Gamma_m(\gamma_p r_0, \gamma_p r)\, \mathrm{d}r. \tag{2.25}$$

In this definition, we have made use of the symmetry inherent in the problem, namely that $\tilde{C}^s_q(r, L) = \tilde{C}^c_q(r, 0)$ and $\tilde{C}^s_q(r, 0) = \tilde{C}^c_q(r, L)$. The integrals (2.25) can be evaluated analytically, from which we arrive at the expressions

$$C^s_{pq} = -\eta_1 r_1 \frac{\bar{\rho}_h}{\bar{\rho}_c} \frac{\Gamma_m(\gamma_p r_0, \gamma_p r_1)\Gamma_m(\gamma_q r_0, \gamma_q r_1)}{\|\Gamma_{m,p}\|^2} \frac{\kappa_q}{L} \sum_{n=-\infty}^{\infty} \frac{\Lambda_n}{(\tilde{\gamma}_n^2 - \gamma_p^2)(\tilde{\gamma}_n^2 - \gamma_q^2)}, \tag{2.26a}$$

$$C^c_{pq} = -\eta_1 r_1 \frac{\bar{\rho}_h}{\bar{\rho}_c} \frac{\Gamma_m(\gamma_p r_0, \gamma_p r_1)\Gamma_m(\gamma_q r_0, \gamma_q r_1)}{\|\Gamma_{m,p}\|^2} \frac{\kappa_q}{L} \sum_{n=-\infty}^{\infty} \frac{(-1)^n \Lambda_n}{(\tilde{\gamma}_n^2 - \gamma_p^2)(\tilde{\gamma}_n^2 - \gamma_q^2)}. \tag{2.26b}$$

These expressions contain a system-dependent factor, Λ_n, for which several forms are provided in § A.4 of the Appendix. Finally, it is useful to rearrange the two sets of algebraic equations, in anticipation of our choice of forcing amplitudes:

$$\frac{\exp(\mathrm{i}\kappa_p L)}{\sin \kappa_p L}\alpha_p^- + \sum_q C^s_{pq}\alpha_q^- + \frac{1}{\sin \kappa_p L}(\beta_p^+ - \beta_p^-) + \sum_q C^c_{pq}(\beta_q^+ - \beta_q^-) = \frac{\exp(-\mathrm{i}\kappa_p L)}{\sin \kappa_p L}\alpha_p^+ + \sum_q C^s_{pq}\alpha_q^+, \tag{2.27a}$$

$$\frac{1}{\sin \kappa_p L}\alpha_p^- + \sum_q C^c_{pq}\alpha_q^- + \frac{1}{\sin \kappa_p L}(\exp(\mathrm{i}\kappa_p L)\beta_p^+ - \exp(-\mathrm{i}\kappa_p L)\beta_p^-) + \sum_q C^s_{pq}(\beta_q^+ - \beta_q^-) = \frac{1}{\sin \kappa_p L}\alpha_p^+ + \sum_q C^c_{pq}\alpha_q^+. \tag{2.27b}$$

Note that when the liners are absent, the coupling matrices are identically zero, and the solution reduces to that for a rigid-walled duct, $\beta_p^+ = \alpha_p^+ \exp(-\mathrm{i}\kappa_p L)$ and $\beta_p^- = \alpha_p^- \exp(\mathrm{i}\kappa_p L)$.

Equations (2.27*a*, *b*) must be closed by specifying two additional constraints to reduce the number of sets of unknown coefficients to two. The first of these constraints is a forcing of the system – by convention we prescribe α_p^+ as the set of incident wave amplitudes (we could easily have chosen β_p^-). For simplicity, we will consider only a single incident mode, α_s^+; because of the linearity of the problem, one mode of unit amplitude is sufficient. Thus,

$$\alpha_p^+ = \begin{cases} 1, & p = s, \\ 0, & p \neq s. \end{cases} \tag{2.28}$$

The incident wave that we choose to prescribe must be cut on (propagating) at the frequency of interest. The criterion for this is $\kappa_s \in \mathbb{R}$, or

$$\omega > \bar{c}_h \gamma_s. \tag{2.29}$$

The second constraint poses a relationship between the transmitted wave amplitudes β_p^+, and the returning wave amplitudes β_p^-. This relationship will clearly depend on the nature of the configuration downstream of the liner system. We will assume a relationship of the form

$$\beta_p^- = \rho_{mp}\beta_p^+ \quad \text{(no sum over } p\text{)}, \tag{2.30}$$

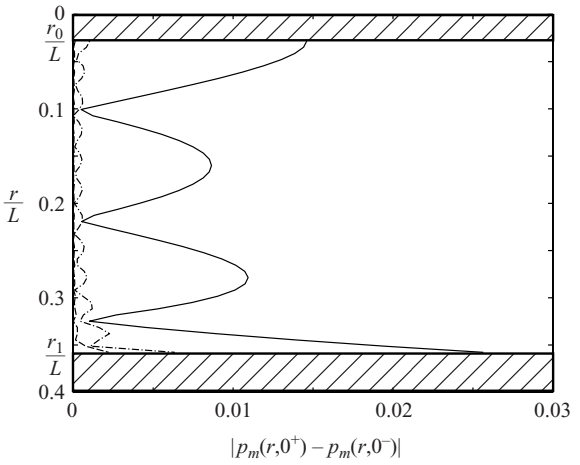

FIGURE 3. Difference in pressure across upstream interface $x = 0$, for the geometry in § 3.3, frequency $kL = 13$ and varying truncation N_r. ——, $N_r = 2$; —·—, $N_r = 10$; — — —, $N_r = 30$.

in which we have made explicit the dependence of the reflection coefficient, ρ_{mp}, on the circumferential mode, m. In this work, we do not attempt to accurately model real configurations, and thus we limit ρ_{mp} to either 0 (corresponding to a semi-infinite downstream duct) or $-\exp(-\mathrm{i}2\kappa_p L_d)$ (approximately corresponding to an open-ended duct of length L_d, ignoring radiation effects). The exception is in § 3.1, in which we use the solution provided by Levine & Schwinger (1948) for the reflection in an unflanged circular duct.

The infinite system of equations (2.27a,b) and (2.30) cannot generally be solved analytically, and two choices of truncation must be made to permit numerical solution. The first choice is the set of radial modes, $p = 0, \ldots, N_r$, to include. The truncated system must include all cuton modes, as well as a sufficient number of cutoff modes, where 'sufficient' is defined as leading to a solution that is invariant (to within desired accuracy) to the inclusion of additional modes. For a given duct, truncation is frequency dependent; for higher frequency, cutoff modes will decay less rapidly and thus a larger number will affect the solution. In figure 3, we present the error between the pressure profiles computed at $x = 0^-$ and $x = 0^+$ for three choices of N_r, for the annular geometry considered in § 3.3. The error at the outer wall does not converge to zero as quickly as in the bulk of the duct, because the finite liner velocity at $(r, x) = (r_1, 0^+)$ requires that the wall-normal pressure derivative be discontinuous across the interface. However, this does not have a significant effect on the overall solution. For example, in the applications presented in this paper in which two radial modes are cut on, we have found good results including 9 cutoff modes (i.e. $N_r = 10$). Also note that the solution remains bounded at $(r, x) = (r_1, 0^+)$, and thus the edge condition of integrable energy density is satisfied.

The second truncation choice is with respect to the infinite series in computing the coupling matrices, C^s_{pq} and C^c_{pq}, in (2.26a) and (2.26b), respectively. This choice is related to the number of cosines we use to approximate the Green's function (or equivalently, the pressure) along the length of the liner, so we label the truncated range as $-N_c \leqslant n \leqslant N_c$. We have already verified that the cosine series expansion of the pressure converges uniformly along the liner. Note that the summand is an even function of n, so that only the non-negative range of indices need be computed. It

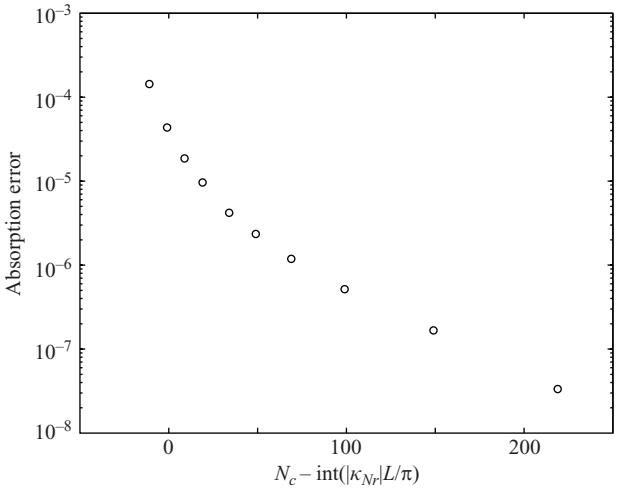

FIGURE 4. Error in absorption computation with varying truncation of cosine series in (2.26*a*) and (2.26*b*). The geometry is from § 3.3 and $kL = 13$.

is easy to verify that the real terms in each summation decay like $O(n^{-4})$ and the imaginary terms like $O(n^{-5})$ as $n \to \infty$. The two factors in the denominator each contribute $O(n^{-2})$ to these overall convergence rates, but only when n is significantly larger than $|\kappa_p|L/\pi$ or $|\kappa_q|L/\pi$, respectively. Thus, convergence will be slower for larger radial mode numbers p and q, above cutoff. Rather than attempt to optimize the truncation for each combination of p and q, however, we choose N_c so that the series corresponding to the largest modes – that is, $(p, q) = (N_r, N_r)$ – are converged below an error threshold. The truncated series are thus extended by an additional $\tilde{N}_c$ terms,

$$N_c = \text{int}(|\kappa_{N_r}|L/\pi) + \tilde{N}_c. \tag{2.31}$$

In figure 4, an overall solution error (based on the acoustic absorption as defined in the next section, and evaluated with respect to a superconverged result) is evaluated for different choices of $\tilde{N}_c$, for one particular geometry and frequency. For an arbitrary error tolerance of 10^{-6}, it is clear that $\tilde{N}_c = 100$ leads to sufficient accuracy. This latter choice was suitable for all cases considered in this work, but is (weakly) problem dependent and should not be considered a general rule.

2.3. *Duct acoustic energy*

In this section we define the acoustic absorption, which we will use as our metric for evaluating the performance of the liner system in § 3. The flux of acoustic energy in the duct is given by

$$I_x = \int_{S_{duct}} \langle p'u' \rangle \, \mathrm{d}S, \tag{2.32}$$

where the integral is over the duct cross-section, and the angled brackets denote an average over time. In a rigid-walled duct, this can be reformulated using the eigenfunction expansions (2.7) and (2.12). Exploiting the orthogonality of these

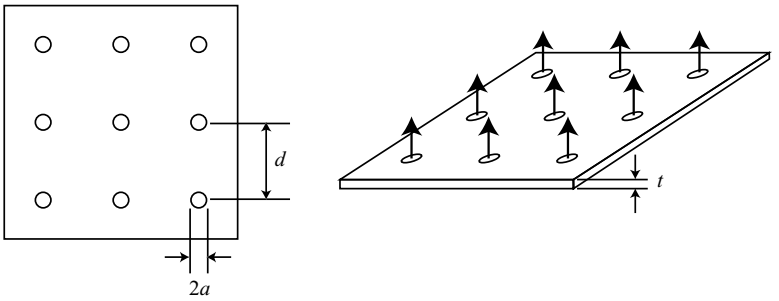

FIGURE 5. Arrangement of apertures in liner.

eigenfunctions, we obtain

$$I_x = \frac{\pi}{\bar{\rho}_h \bar{c}_h} \sum_{q=0}^{N_{max}} \frac{\mathrm{Re}(\kappa_q)}{k_h} (|\alpha_q^+|^2 - |\alpha_q^-|^2) \|\Gamma_{m,q}\|^2 + \frac{\pi}{\bar{\rho}_h \bar{c}_h} \sum_{q>N_{max}} \frac{2\mathrm{Im}(\kappa_q)}{k_h} \mathrm{Im}(\alpha_q^{+*} \alpha_q^-) \|\Gamma_{m,q}\|^2, \tag{2.33}$$

where $()^*$ denotes complex conjugate. The first term contains all cuton modes, and the second consists of the remaining cutoff modes. This second sum contains some energy, but is generally negligible because either the right- or left-travelling wave amplitude is exponentially small.

We define the acoustic absorption, Δ, as the fraction of propagating duct energy that enters the lined section that does not exit it. As described in § 2.2, we restrict our attention to incident waves containing only a single mode (m, s) of unit amplitude. Thus, the absorption is defined as

$$\Delta \equiv 1 - \frac{\displaystyle\sum_{q=0}^{N_{max}} \frac{\kappa_q}{\kappa_s} (|\alpha_q^-|^2 + |\beta_q^+|^2) \frac{\|\Gamma_{m,q}\|^2}{\|\Gamma_{m,s}\|^2}}{\displaystyle 1 + \sum_{q=0}^{N_{max}} \frac{\kappa_q}{\kappa_s} |\beta_q^-|^2 \frac{\|\Gamma_{m,q}\|^2}{\|\Gamma_{m,s}\|^2}}, \tag{2.34}$$

where it is understood that the axial wavenumbers are purely real for all terms.

2.4. *Liner compliance*

Our development thus far has left the acoustic properties of the liner completely unspecified. We now specialize the analysis to a thin liner comprised of a homogeneous array of circular apertures, through each of which a mean flow issues (see figure 5). Provided that the distance between apertures, d, is much larger than their individual radii, a, then the acoustic behaviour of each aperture can be treated in isolation. This restriction can be expressed in terms of the open-area ratio of the liner, σ, as

$$\sigma = \frac{\pi a^2}{d^2} \ll 1. \tag{2.35}$$

Note that the first equality is only valid if the apertures are arranged on a Cartesian grid with spacing d in both directions. This configuration is chosen for simplicity, though other arrangements are certainly admissible, and the conclusions drawn in this work are generally applicable to all regular arrays with constant d. Furthermore,

if d is small compared with the acoustic wavelength, then the liner characteristics can be regarded as a homogeneous composition of the individual aperture properties.

In previous work (Hughes & Dowling 1990; Eldredge & Dowling 2003), these assumptions allowed the development of a liner compliance from the Rayleigh conductivity, K_a, of a single aperture through which a high-Reynolds-number flow passes, derived by Howe (1979). The conductivity accounts for the absorption inherent in vorticity shed periodically from the rim of the aperture owing to the fluctuating pressure across it. The acoustic volume flux through the aperture can be distributed over the surrounding cell of side d to provide the effective compliance. This compliance can be modified to include the inertia of the fluid within the thickness of the liner, t. The result, which we merely quote here, is

$$\frac{1}{\eta} = \frac{\pi a^2}{\sigma}\frac{1}{K_a} + \frac{t}{\sigma}, \tag{2.36}$$

where K_a is given by

$$K_a = 2a(\gamma + \mathrm{i}\delta). \tag{2.37}$$

The components γ and δ are only functions of the Strouhal number, St, which is approximately given by

$$St \approx ka/M_h, \tag{2.38}$$

where M_h is the Mach number of the mean aperture flow. These functions are given by equations (3.14) of Howe (1979). Note that the sign of the imaginary part differs from that of Howe because of the convention of using $\exp(\mathrm{i}\omega t)$ here. It should be noted that δ is always positive, so that energy is only absorbed by the liner in this model, and can never be generated.

3. Results

3.1. *Comparison with one-dimensional model*

In previous work (Eldredge & Dowling 2003), we developed a one-dimensional model for the absorption of planar acoustic waves in a duct. The analysis was simplified by assuming that the fluctuating pressure consisted entirely of plane waves in the rigid-walled ducts, the lined section, and the cavities. This is not strictly true in any region: in the rigid-walled ducts, evanescent waves with radial variation will be present just upstream and downstream of the liner; in the lined section and cavities, the normal derivative of the pressure must be non-zero at the liner to balance the acoustic velocity through it. However, for small compliances and frequencies below the cuton of higher-order modes it is reasonable to ignore these effects, and the excellent agreement of the model with experimental results supported these approximations.

Here we evaluate this approach by comparing the results for a planar incident wave, using both the present model and the one-dimensional model. This comparison is illustrated in figure 6, which shows the absorption computed by both models for a double liner system with open-ended downstream duct section (of length $L_d/L = 4.5$), versus the scaled frequency, kL (the mean temperatures are equal, so $k_h = k_c = k$). The duct is cylindrical, with $r_1/L = 0.358$, $r_2/L = 0.428$, $\sigma_1 = 0.0398$, $t_1/L = 0.0237$, $\sigma_2 = 0.0198$ and $t_2/L = 0.0169$. The aperture Mach number in the innermost liner is $M_{h,1} = 0.023$. The results are nearly indistinguishable from each other, except at larger frequencies where there is slight disagreement at the absorption troughs. The strong similarity of these results verifies the one-dimensional approach for frequencies

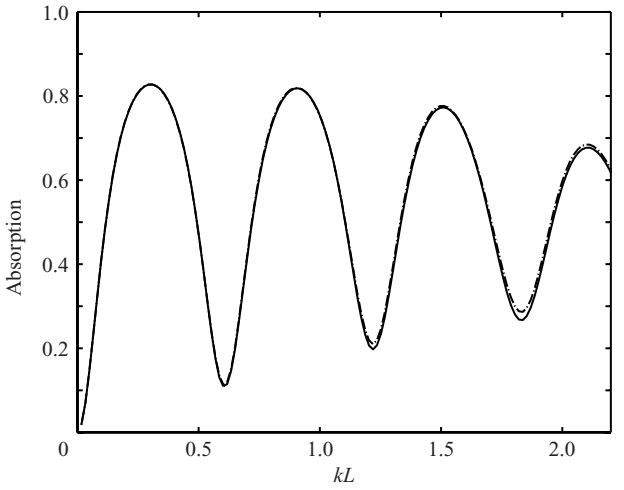

FIGURE 6. Comparison of absorption from double liner system with open downstream end. ——, present model; —·—, one-dimensional model.

below the cuton of higher modes; the evanescent waves scattered by the duct/liner interface have little effect, as does the small radial variation adjacent to the liner.

It was explained in Eldredge & Dowling (2003) that the absorption troughs in figure 6 are due to the presence of a pressure node near the middle of the lined section of duct, which limits the energy flux through the liner and hence reduces the absorption. This behaviour will be examined in more detail in the next section.

3.2. *Higher circumferential modes*

We next consider the interaction of incident modes that have circumferential variation, but which are fundamental in the radial direction (i.e. using the terminology of § 2.2, $m \neq 0$, $s = 0$). In an annular geometry in which the transverse duct dimension is small compared with the radius, such modes travel through the rigid-walled duct in a helical pattern, approximately parallel to the walls. Thus, it is reasonable to expect that they will interact with the liner in a similar way to plane waves, since they can be classified in the same category of 'grazing modes'.

In fact, this behaviour can be revealed by averaging equation (2.1) over a narrow annular region, $r \in [r_1(1-\epsilon), r_1]$, where $\epsilon \ll 1$. The resulting equation for the radially averaged pressure is,

$$\frac{\mathrm{d}^2 \bar{p}_m}{\mathrm{d}x^2} + \left(k^2 - \frac{m^2}{r_1^2}\right) \bar{p}_m = -\frac{1}{\Delta r} \left.\frac{\partial p_m}{\partial r}\right|_{r_1} + O(\epsilon), \tag{3.1}$$

where $\Delta r = \epsilon r_1$ and $\bar{p}_m$ is defined as

$$\bar{p}_m(x) \equiv \frac{1}{r_1 \Delta r} \int_{r_1(1-\epsilon)}^{r_1} r p_m(r, x)\, \mathrm{d}r. \tag{3.2}$$

We have also assumed that no mean temperature differences are present, so $k_h = k_c = k$. A wall compliance condition (e.g. equation (2.4)) can be used to replace the radial derivative of the pressure at the lined wall in (3.1). It is consistent with our previous approximations to replace the jump in local pressures across the liner with the difference in averaged pressures on either side of the liner. The result, omitting

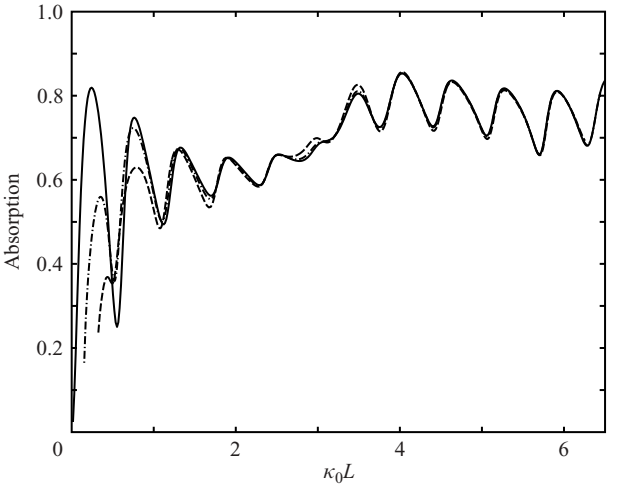

FIGURE 7. Absorption of incident modes versus axial wave vector component in annular duct. ——, $m = 0$; —·—, $m = 1$; — — —, $m = 2$.

the error term, is

$$\frac{\mathrm{d}^2 \bar{p}_m}{\mathrm{d}x^2} + \left(k^2 - \frac{m^2}{r_1^2}\right) \bar{p}_m = \frac{\eta_1}{\Delta r}(\bar{p}_m - \bar{p}_{m,c}), \tag{3.3}$$

which is a wave equation for the radially averaged pressure, with a coupling with the averaged pressure in the adjacent cavity, $\bar{p}_{m,c}$ (for which we can derive a similar wave equation).

When $m = 0$, this equation is essentially the basis for the one-dimensional model of Eldredge & Dowling (2003). Higher circumferential modes only serve to modify the axial wavenumber, and for small annular gap, results for different modes that have the same axial wavenumber should be comparable. This is clearly exhibited in figure 7, where the absorption of the $m = 0$, 1 and 2 modes by a double-liner system in an annular duct is plotted versus the axial wavenumber, $\kappa_0 L$, which is given approximately by

$$\kappa_0 L \approx kL \left(1 - \frac{m^2}{k^2 r_1^2}\right)^{1/2}. \tag{3.4}$$

The parameters are $r_0/L = 1.10$, $r_1/L = 1.13$, $r_2/L = 1.18$, $\sigma_1 = 0.0398$, $t_1/L = 0.0237$, $\sigma_2 = 0.0198$, $t_2/L = 0.0169$ and $M_{h,1} = 0.108$. The duct is open-ended, with downstream length $L_d/L = 4.5$. The full model was used to compute the results. At small axial wavenumbers, the agreement is poor because the liner compliance is dependent on the full wave vector magnitude (through its Strouhal number dependence) rather than just its axial component. As the wave vectors of the $m = 1$ and $m = 2$ modes are skewed further from the duct axis as $\kappa_0 L \to 0$, the wave vector magnitudes (and hence Strouhal numbers) of the three modes are sharply different.

As the axial wavenumber grows, it becomes comparable to and then surpasses the circumferential component of the wave vector. The scaled results for both higher circumferential modes become very similar to the plane-wave results when the axial component is the larger of the two. For $m = 1$, this cross-over corresponds to $\kappa_0 L \gtrsim 0.89$, and for $m = 2$, $\kappa_0 L \gtrsim 1.78$. The results are nearly indistinguishable from each other in these ranges.

The self-similarity of the results for higher circumferential modes in a thin annular duct allows us to adopt the design rules developed in Eldredge & Dowling (2003) for maximizing the peak absorption of incident plane waves in a lined duct with a strongly reflective downstream configuration. These design rules prescribed an optimal relationship between the parameters of the system of

$$\left(\frac{M_{h,1}}{\sigma_1}\right)_{opt} = \frac{1}{2\sqrt{2}}\frac{C_1 L}{S_p}, \tag{3.5}$$

for a single liner, where C_1 is the circumference of the liner, $C_1 = 2\pi r_1$, and S_p is the duct cross-sectional area, $S_p = \pi(r_1^2 - r_0^2)$. For a double liner, the peaks are maximized when

$$\left(\frac{M_{h,1}}{\sigma_1}\right)_{opt} = \frac{1}{2\sqrt{2}}\frac{C_1 L/S_p}{(\sigma_1/\sigma_2)^2(C_1/C_2)^2 + 1}, \tag{3.6}$$

where C_2 is the circumference of the outer liner.

These criteria require no modification to optimize the liner system for higher circumferential modes. Though it is apparent from figure 7 that the peak absorption for both $m = 1$ and $m = 2$ strays from the predicted optimum as the axial wave vector component approaches zero, the range in frequency, kL, over which this deviation occurs is smaller (in fact, it is only $\sqrt{2} - 1 \approx 0.41$ of the corresponding range of axial wavenumbers).

Note the change in character of the absorption plot of figure 7 for axial wavenumber larger than approximately 3. This behaviour can be explained by considering the reflection of waves from the open duct end. Such a reflection is nearly perfect (indeed, in our modelling, $|\rho_{m0}| = 1$), leading to standing waves in the downstream section of duct, and possibly the presence of pressure nodes in the lined section. The effect of pressure nodes is demonstrated by solving the simpler problem of a plane wave interacting with a single liner. The results of this interaction are depicted in figure 8, for an annular duct with $r_0/L = 0.282$, $r_1/L = 0.358$, $\sigma = 0.0398$ and $M_h = 0.207$. The central absorption plot is surrounded by profiles of the axial distribution of energy flux through the liner at several frequencies. The energy flux is normalized by the incident duct energy so that the integral under each curve is equal to the total absorption.

For frequencies such that $\kappa_0 L < \pi$, the liner supports less than half of a wavelength, and thus no pressure nodes are present in certain frequency ranges, such as those centred at $\kappa_0 L = 0.31$ and 0.89. In these ranges, the energy flux is distributed nearly uniformly across the liner, and the absorption achieves a relative maximum. In contrast, half wavelengths also permit the presence of a single pressure node, and the absorption is smallest when this node is near the centre of the lined section, where it has the greatest effect on limiting the liner energy flux, as at $\kappa_0 L = 0.60$ and 1.20. The effect of the node is diminished and the absorption troughs are shallower at larger axial wavenumber as the liner is able to support more substantial portions of the energy flux on either side of the node.

In the range $\pi < \kappa_0 L < 2\pi$, at least one pressure 'node' is always present. Relative absorption maxima, such as at $\kappa_0 L = 4.24$ and 4.85, correspond to the node situated near the centre of the liner, allowing peaks in the energy flux on either side. Relative minima, for example at $\kappa_0 L = 4.53$ and 5.15, coincide with two nodes evenly distributed in the section. However, the difference in absorption between peak and trough in this frequency range is very slight, because the energy flux distribution is nearly unchanging apart from a shift in phase. The benefit of the downstream reflection is thus greatly diminished at frequencies for which $\kappa_0 L > \pi$, as is evident by comparing with the

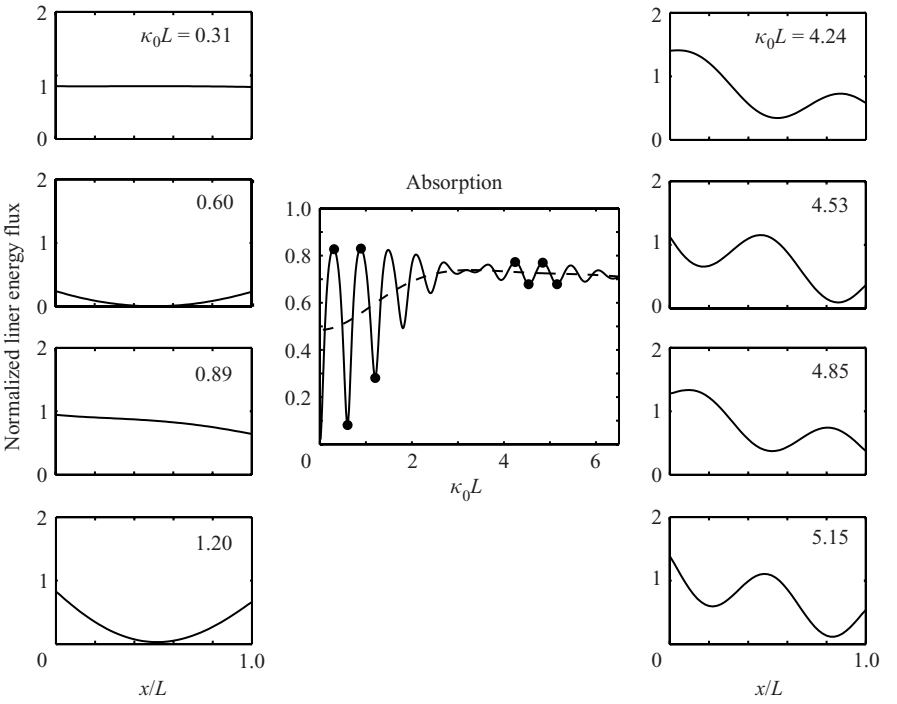

FIGURE 8. Normalized energy flux through liner versus axial position at several axial wavenumbers, denoted by ● on central absorption plot. Planar mode in annular duct interacting with a single-liner system. ——, open-ended duct; — — —, semi-infinite duct.

included plot of absorption with a semi-infinite downstream duct in figure 8; the difference in absorption between the two cases is much less remarkable in this range.

3.3. *Higher radial modes*

The analyses of the previous two sections focused on ranges of frequency over which the acoustic wavelength was comparable to the duct and liner lengths, yet significantly larger than any radial dimension. Consequently, they revealed behaviour that was relatively independent of the transverse extent of the system. At higher frequencies, however, the width of duct and cavities become important, and if a larger range of frequency is considered, the effect of the radial dimension becomes clear. In particular, resonances in the duct and liner cavities can lead to enhanced absorption at certain frequencies. These resonances are embodied in the decoupling Green's function, and specifically in the poles of the system factor Λ_n present in the coupling matrices (2.26*a*) and (2.26*b*). In this section, we explore the effect of liner system resonances on axisymmetric incident modes. To simplify matters, we will eliminate one axial dimension by making the downstream duct semi-infinite, thus preventing the absorption peaks and troughs due to reflection.

Consider an annular duct with a single liner surrounded by a hollow cavity formed by a rigid outer wall. The inner wall is at radius $r_0/L = 0.0282$, the liner and outer duct wall are at $r_1/L = 0.358$, and the radius of the outer cavity wall is variable. The liner open-area ratio is $\sigma = 0.0398$, the aperture radius is $a/L = 2.11 \times 10^{-3}$ and the liner thickness is $t/L = 0.0237$. The bias flow is set at $M_{h,1} = 0.05$. In figure 9, an example pressure profile at $x = 0$ is depicted for dimensionless frequency $kL = 13$ ($\kappa_1 L = 7.08$)

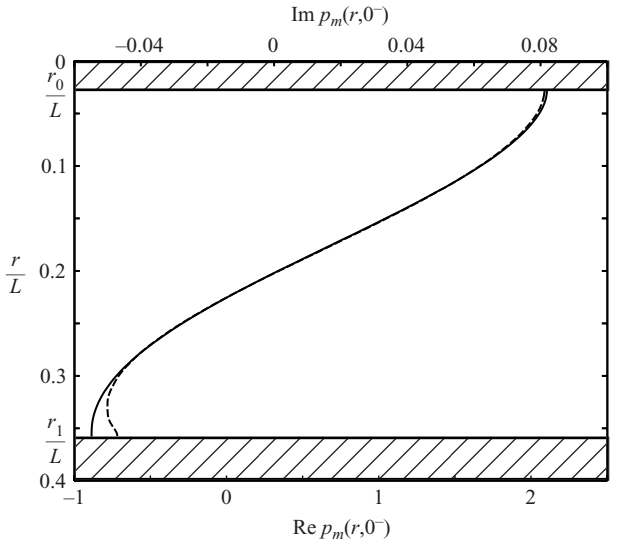

FIGURE 9. ——, real and − − −, imaginary components of pressure at interface $x = 0$ for $r_2/r_1 = 1.67$ and $kL = 13$.

and $r_2/r_1 = 1.67$ when the incident wave consists of the first axisymmetric radial mode $(m, s) = (0, 1)$. Note the different scales used to depict the real and imaginary parts.

The absorption for the same incident mode is depicted in figure 10 at varying frequency (represented by the axial wavenumber, $\kappa_1 L$), beginning with the cuton frequency of the mode. The acoustic wavelength is much larger than the aperture pitch over the entire frequency range considered, $kd < 0.3$. In each successive plot, the rigid cavity wall is brought further inward, thereby decreasing the cavity depth.

Several peaks can be observed, each of which corresponds to a resonance in the liner system. To understand the physical significance of these resonances, it is instructive to examine the poles of Λ_n for this system, given by (A 27), which for uniform mean temperatures can be written as

$$\Lambda_n = -\frac{D^{(0)'}_{n,<}(\tilde{\gamma}_n r_0, \tilde{\gamma}_n r_1) D^{(1)'}_{n,>}(\tilde{\gamma}_n r_2, \tilde{\gamma}_n r_1)}{D^{(0)'}_{n,<}(\tilde{\gamma}_n r_0, \tilde{\gamma}_n r_1) D^{(1)'}_{n,>}(\tilde{\gamma}_n r_2, \tilde{\gamma}_n r_1) - \dfrac{\eta_1}{\tilde{\gamma}_n} \dfrac{2}{\pi \tilde{\gamma}_n r_1} D^{(0)'}_{n,<}(\tilde{\gamma}_n r_0, \tilde{\gamma}_n r_2)}. \tag{3.7}$$

Poles and zeros occur in pairs in this function, and there are three types of each. The first type of zero arises from solutions of the duct equation

$$D^{(0)'}_{n,<}(\gamma r_0, \gamma r_1) = 0, \tag{3.8}$$

which we write as $\gamma = \zeta^{(0)}_p$. There is no dependence on n, because (3.8) does not contain a compliance, and is thus independent of frequency (recall that $k^2 = \tilde{\gamma}_n^2 + n^2\pi^2/L^2$). Indeed, this countably infinite set of zeros is simply the set of radial eigenvalues of the rigid annular duct. Near these zeros, Λ_n can be written as

$$\Lambda_n = \frac{D^{(0)'}_{n,<}(\tilde{\gamma}_n r_0, \tilde{\gamma}_n r_1)}{B^{(0)}_n} + O\left(\tilde{\gamma}_n - \zeta^{(0)}_p\right)^2. \tag{3.9}$$

Thus, the set of poles $\pi^{(0)}_{n,p}$ are the zeros of $B^{(0)}_n$, which differ from the zeros $\zeta^{(0)}_p$ by a small amount that depends on the compliance, and therefore n.

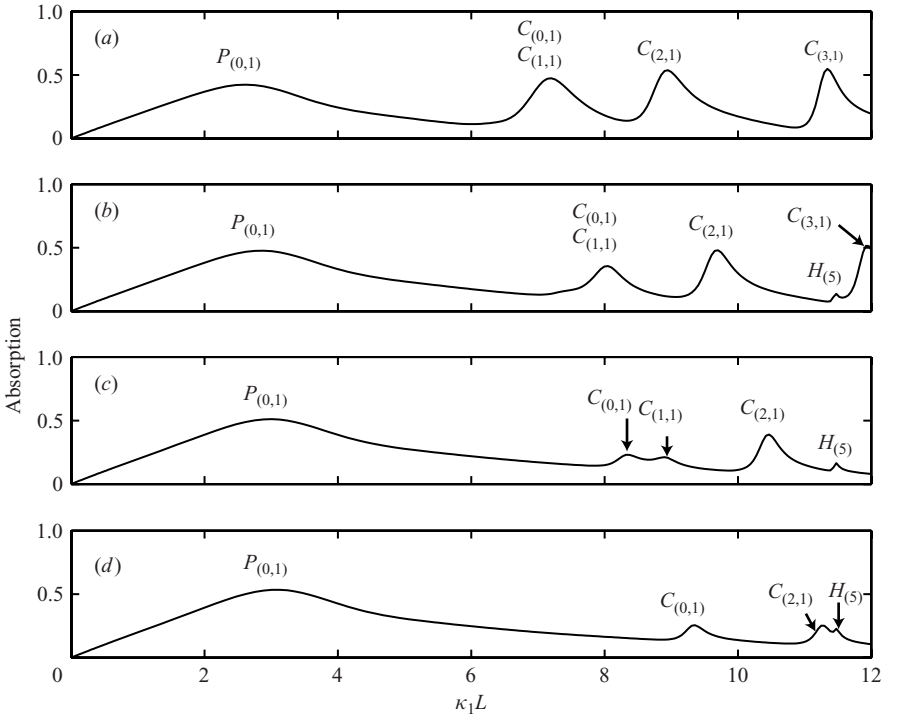

FIGURE 10. Absorption of first radial mode by liner with rigid-walled cavity, with varying cavity depth. P, duct resonances; C, cavity; H, Helmholtz. (*a*) $r_2/r_1 = 1.73$, (*b*) $r_2/r_1 = 1.70$, (*c*) $r_2/r_1 = 1.67$, (*d*) $r_2/r_1 = 1.64$.

It is clear that this set of poles corresponds to resonances in the lined section of duct, and we label them P (for 'pipe'). However, only the frequencies associated with $n = 0$ lead to physically realizable resonances, because there are no walls to support higher cosine modes in x. The higher n solutions are poles of the Green's function only because its derivatives are constrained to vanish at $x = 0, L$; the pressure is not so constrained. The complex frequencies at which the resonances occur are thus given by

$$k_{0,p}^{(0)} = \pi_{0,p}^{(0)}. \tag{3.10}$$

Note that the right-hand side has some dependence on frequency through the compliance, so this is not an explicit expression for the complex frequency. However, the dependence is very weak and an iterative solution is straightforward. Real forcing frequencies that lie near $\mathrm{Re}(k_{0,p}^{(0)})$ will lead to large responses by the system. Because $k_{0,p}^{(0)} \approx \zeta_p^{(0)}$, the associated resonance $P_{(0,p)}$ occurs very near the cuton frequency of duct mode p, though it is generally only substantial when mode p is present in the incident wave. Near cuton, the incident wave is bouncing between the inner and outer walls of the duct with very little propagation in the axial direction. In the lined section, these waves impinge almost normally on the liner and are thus able to excite large responses. This is evident in all plots of figure 10 in the wide peak near $\kappa_1 L = 3$, labelled $P_{(0,1)}$. The width of the peak is somewhat misleading, because the axial wavenumber becomes very sensitive to frequency as $\kappa_1 L \to 0$; the frequency bandwidth of the peak is much smaller. This sensitivity near cuton also explains the

visible drift of the peak as the cavity is made shallower, as the slight dependence of the duct resonance on the cavity behaviour is amplified.

The second type of zero/pole of Λ_n is due to roots of the cavity equation

$$D^{(1)'}_{n,>}(\gamma r_2, \gamma r_1) = 0, \tag{3.11}$$

denoted by $\gamma = \zeta^{(1)}_p$. Near these zeros, Λ_n reduces to

$$\Lambda_n = -\frac{D^{(1)'}_{n,>}(\tilde{\gamma}_n r_2, \tilde{\gamma}_n r_1)}{B^{(1)}_n} + O\left(\tilde{\gamma}_n - \zeta^{(1)}_p\right)^2, \tag{3.12}$$

and thus this set of poles $\pi^{(1)}_{n,p}$ is given by the zeros of $B^{(1)}_n$, distinct from the corresponding $\zeta^{(1)}_p$ by a small compliance correction. This set of poles represents the resonances of the cavity behind the liner (type C). However, in contrast to the previous case, the rigid walls that form the ends of the cavity allow higher axial cosine modes, so the frequencies at which observable resonances occur are given by

$$k^{(1)}_{n,p} = \left(\pi^{(1),2}_{n,p} + \frac{n^2\pi^2}{L^2}\right)^{1/2}. \tag{3.13}$$

Again, this should be treated as an implicit expression for the complex frequency. In figure 10(a), the single peak at $\kappa_1 L = 7.2$ corresponds to both resonances, $C_{(0,1)}$ and $C_{(1,1)}$, associated with closely spaced frequencies $k^{(1)}_{(0,1)}$ and $k^{(1)}_{(1,1)}$. The next two peaks at $\kappa_1 L = 9$ and $\kappa_1 L = 11.3$ coincide with resonant modes $C_{(2,1)}$ and $C_{(3,1)}$, respectively. As the rigid outer wall is brought nearer the liner, the real parts of the poles $\pi^{(1)}_{n,p}$ are increased, and thus the peaks shift to higher frequencies. In figure 10(c), the $C_{(0,1)}$ and $C_{(1,1)}$ peaks are now distinct, though significantly smaller. In figure 10(d), the $C_{(1,1)}$ peak is no longer visible above the background absorption level.

The third and final type of pole of Λ_n for this system is affiliated with the trivial zeros,

$$\tilde{\gamma}_n = 0. \tag{3.14}$$

In contrast with the previous two types, this set has only a single member for each n. Equation (3.7) can be expanded about this zero, and for circumferential mode $m = 0$ the affiliated pole is approximately

$$\pi^{(h)} = \left[2\eta_1 r_1 \left(\frac{1}{r_1^2 - r_0^2} + \frac{1}{r_2^2 - r_1^2}\right)\right]^{1/2}. \tag{3.15}$$

This pole corresponds to Helmholtz resonance of the liner system (type H). The cavity and lined section of duct act in tandem as resonators, providing stiffness to the fluctuating flow through the apertures in the liner with effective neck length σ/η_1 and orifice area $2\pi r_1 \sigma$. The corresponding complex frequencies are given by iterative solution of

$$k^{(h)}_n = \left(\pi^{(h),2} + \frac{n^2\pi^2}{L^2}\right)^{1/2}, \tag{3.16}$$

and represent Helmholtz resonance in the radial direction coupled with axial cosine modes in the cavity. This type of resonance was also identified by Hughes & Dowling (1990) in the context of waves incident upon liners and screens. However, their investigation focused on cavities that were much shallower than the duct radius, so that their so-called 'resonance parameter', Q, was only dependent on the cavity depth.

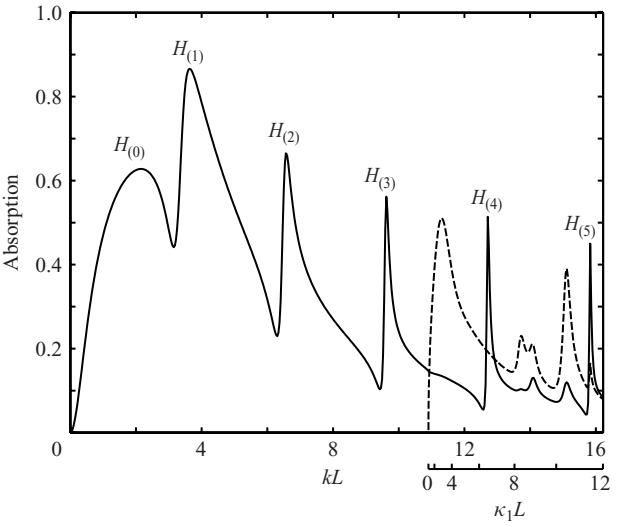

FIGURE 11. Absorption of different modes by single liner/cavity system, $r_2/r_1 = 1.67$, semi-infinite downstream duct. ——, $s = 0$; — — —, $s = 1$. An additional axis corresponding to the axial wavenumber of the first radial mode is included for comparison with figure 10(*c*).

The poles given by (3.15) reduce to their $Q = 1$ condition for shallow cavity and large Strouhal number (and infinitesimally thin liner).

In the case considered in figure 10, excitation of Helmholtz-type resonance is limited owing to the radial component of the incident mode (the resonance is most effective when there is little radial variation, so that the resonator volume is uniformly stiff, as will be demonstrated below). Thus, the absorption at most values of n is not enhanced above the background level. However, the small peak at $\kappa_1 L = 15.8$, labelled as $H_{(5)}$ in figure 10(*b–d*), corresponds to Helmholtz resonance with $n = 5$. As frequency increases, the resistance of the liner is diminished because successive vortex rings shed by each aperture are more closely spaced, which tends to cancel their induced velocities at the aperture rim. Simultaneously, the reactance of the liner approaches a constant level dominated by the inertia of the fluid within its thickness. This behaviour has the dual effect of suppressing the background level of absorption, and sharpening the Helmholtz resonance peaks obtainable by real frequencies, as the complex frequency is now brought nearer the real axis. Furthermore, a notable portion of the incident wave is scattered into plane waves at the frequency where the peak is observed, and thus Helmholtz resonance is a secondary effect achieved by these scattered waves. Note that the absorption peak does not shift substantially with decreasing cavity depth, because the cross-sectional area of the cavity is nearly twice that of the duct, so the latter area dominates the determination of the frequency in (3.15).

As described above, the Helmholtz-type resonance of the liner system is most notable when the incident wave has little radial dependence, as in a plane wave. This is clearly demonstrated in figure 11, where the absorption of $s = 0$ and $s = 1$ incident waves by the liner system is compared. Whereas the $s = 1$ mode excites substantial resonances of the duct and cavity, the $s = 0$ mode is dominated by Helmholtz-type resonances corresponding to all values of n (though the peak labelled $H_{(0)}$ is combined with resonances $P_{(0,0)}$ and $C_{(0,0)}$). Small peaks can also be observed at the frequencies corresponding to cavity resonances $C_{(0,1)}$, $C_{(1,1)}$ and $C_{(2,1)}$, but these are secondary resonances due to scattering of the plane wave into the first radial mode

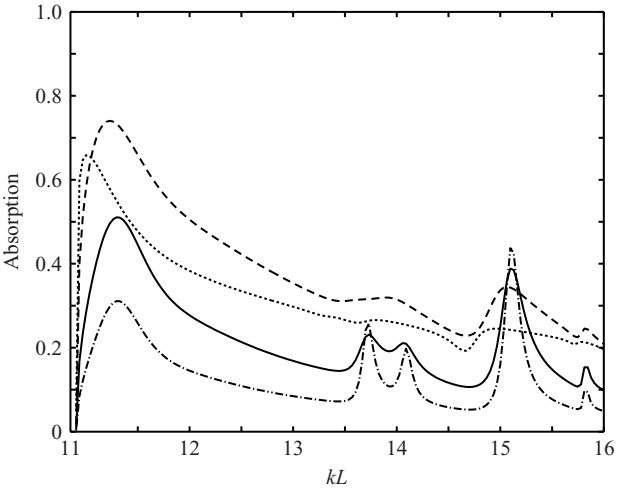

FIGURE 12. Absorption of $s=1$ mode with varying mean aperture flux. —·—, $M_h=0.025$; ——, $M_h=0.05$; – – –, $M_h=0.15$; · · ·, $M_h=0.5$.

at these frequencies, so their effect on the absorption is much weaker than in the $s=1$ incident mode. Note that no peak is discernible in the $s=0$ case at the duct resonance frequency, $k_{0,1}^{(0)}$.

These three types of resonances – duct resonance (P), cavity resonance (C) and Helmholtz resonance (H) – will generally be possible in all liner systems. They can also be excited by incident waves with higher circumferential modes. Whether or not they are actually observed will depend on the nature of the system as well as the incident wave.

It is interesting to consider the effect of changing the bias flow. The resulting absorption of the $s=1$ mode for the liner system with $r_2/r_1=1.67$ is depicted in figure 12, in which the results for four different mean aperture flows are presented versus frequency, kL, rather than axial wavenumber. It should be noted that the highest Mach number presented, $M_h=0.5$, is probably too large for the results to be valid, since the compliance was derived with the assumption that the local aperture flow could be treated as incompressible; we include it here for demonstration purposes only. It is apparent that the response of the incident wave is sensitive to the variation in mean flow. The broadband level of absorption has been raised as M_h has increased up to 0.15, thereby obscuring the resonance peaks. For larger aperture flow, the absorption level is diminished, suggesting that an optimal flow rate exists.

We propose an expression for this optimal flow rate. Absorption is generally larger near frequencies at which the imaginary component of the liner compliance, the liner 'resistance', achieves a maximum. For very thin liners, this maximum occurs at aperture Strouhal number, $St=1.12$. However, for most liners, $t/a>1$, and thus the optimal flow rate is dependent on the fluid inertia provided by the liner thickness. The aperture Strouhal number for liners is often limited to $St \lesssim 1$ (it never exceeds 1.4 in the results presented), for which the Rayleigh conductivity is approximately given by $K_a \approx 2a(St^2/3 + i\pi St/4)$. The imaginary part of the liner compliance provided by (2.36) is therefore nearly

$$\mathrm{Im}(\eta) \approx \frac{1}{2}\frac{\sigma}{a} St \left[1 + \left(\frac{4}{3\pi}\frac{t}{a} + \frac{1}{4}\frac{t^2}{a^2}\right) St^2\right]^{-1}. \tag{3.17}$$

The maximum of this expression occurs at

$$St_{max} \approx \left(\frac{4}{3\pi} \frac{t}{a} + \frac{1}{4} \frac{t^2}{a^2} \right)^{-1/2}, \tag{3.18}$$

or in terms of frequency,

$$(kL)_{max} \approx \frac{M_h}{a/L} \left(\frac{4}{3\pi} \frac{t}{a} + \frac{1}{4} \frac{t^2}{a^2} \right)^{-1/2}. \tag{3.19}$$

Thus, the bias flow exerts a direct influence on the position of the peak resistance. For the case presented in figure 12, the aperture Mach numbers 0.025, 0.05, 0.15 and 0.5 lead to peaks at $(kL)_{max} = 1.97$, 3.94, 11.8 and 39.4, respectively. Thus, only the aperture flow with $M_h = 0.15$ places this peak in the depicted frequency range, and the general level of absorption is relatively larger.

The peak liner resistance played no significant role in determining the optimal absorption for frequencies $kL < \pi$, as considered in §§ 3.1 and 3.2. Rather, the quasi-steady limit $kL \to 0$ was used by Eldredge & Dowling (2003) to derive optimal parameters for maximizing the absorption peaks produced by downstream reflection. The optimal flow rates determined by these different approaches are generally discordant, and the choice of which design approach to use should be guided by the intended use of the liner system.

4. Conclusions

In this work, we have explored the three-dimensional interaction of linear acoustic disturbances in cylindrical and annular ducts with a perforated liner system with bias flow. These finite-length systems may consist of multiple concentric liners, each of which contains a homogeneous array of circular apertures through which the mean flow travels. The fluctuating pressure adjacent to each aperture excites the unsteady shedding of vorticity from its rim, which is convected away by the mean flow and dissipated into heat. This process, when distributed over many such apertures, can remove a significant amount of acoustic energy from the system.

For the analysis of these systems we have developed a decoupling Green's function that recasts the governing Helmholtz equation in integral form, consisting only of surface integrals over the duct interface cross-section. The mechanism of vorticity production is formulated in an effective compliance for each liner; the effects of liners and cavities are embodied in the Green's function, and solution for the amplitudes of scattered modes is straightforward after projecting the integral equation onto the modal eigenfunctions.

In previous work (Eldredge & Dowling 2003), we developed a one-dimensional model for liner systems of this type to investigate the absorption of plane waves at frequencies below the cuton of higher modes. Though this model ignored radial variation in the lined section and evanescent waves at the duct/liner interface, its results compared very well with experiment. With our present model we have verified that the one-dimensional approach is very accurate for a wide range of frequencies. Indeed, the one-dimensional analysis was shown to be equally valid for higher circumferential modes in narrow annular ducts, in which the nearly planar wavefronts travel in a spiralling pattern, but still parallel to the liner. A comparison between different modes revealed self-similar behaviour at common axial wavenumber, and thus the optimal liner design of Eldredge & Dowling (2003) is equally effective for maximizing the absorption of all such 'grazing' modes.

The absorption of acoustic energy associated with these grazing modes is enhanced in certain frequency bands when the downstream geometry reflects a substantial portion of the transmitted energy to further interact with the liner system. For frequencies such that the wavelength is larger than twice the liner length, this enhancement can be substantial if the geometry and flow are nearly optimal. However, the enhancement is greatly diminished for larger frequencies, for which pressure minima are constantly present along the liner.

Over a wider frequency spectrum, transverse effects become much more apparent. Analysis of the poles of the Green's function revealed three classes of resonance – duct, cavity and Helmholtz-type – that can significantly enhance the absorption of incident modes near the associated frequencies. The Helmholtz class of resonance has been previously explored by Hughes & Dowling (1990), who identified the cavity volume as providing stiffness to the fluctuating liner flow; our analysis has shown that, in fact, both the cavity and duct volume act in tandem, though the former is typically smaller and thus dominant. The other two classes of resonance have received little attention in the literature, however. The duct resonance is inextricably connected to the transverse dimensions of the duct, and thus may be difficult to optimize. The cavity resonances, which occur for each longitudinal cosine mode, are very sensitive to both cavity depth and length, and thus it may be possible to incorporate them in the design process. We have also demonstrated that the broadband level of absorption can be maximized in a frequency range by situating within it the peak of the liner resistance.

In future work, we will explore the effect of temperature on the phenomena detailed in this paper. Also, we plan to investigate acoustic interactions in liner systems in the presence of non-negligible duct flow. This problem is significantly more challenging, owing to the potential of triggering instabilities that may generate sound.

This work was conducted while the author was a postdoctoral research associate under the PRECCINSTA project, which was sponsored by the Fifth European Community Framework Programme, Contract no. ENK5-CT2000-00060. The author is especially indebted to Professor Ann Dowling, whose support and counsel have made this work possible.

Appendix. The decoupling Green's function

In this section, our goal will be to develop a Green's function that decouples the integral equation for the pressure in the duct from the pressures in the liner cavities. We begin by developing a set of coupled integral equations for the pressure in each region, eliminating as many boundary integrals as possible through conditions on the corresponding Green's function in that region. We then combine the resulting integral equations to eliminate all cavity pressures. The result of this procedure will be a single 'decoupling' Green's function, through which the pressure in the lined section of duct is determined entirely by its normal derivatives on the upstream and downstream interfaces.

A.1. *Set of integral equations*

Suppose that $G_m^{(0)}$ satisfies the same equation as p_m in Ω_0, but subject to a singular forcing term at $(r', x') \in \Omega_0$:

$$\frac{1}{r}\frac{\partial}{\partial r}\left(r\frac{\partial G_m^{(0)}}{\partial r}\right) + \frac{\partial^2 G_m^{(0)}}{\partial x^2} + \left(k_h^2 - \frac{m^2}{r^2}\right) G_m^{(0)} = \frac{1}{r'}\delta(r - r')\delta(x - x'). \qquad \text{(A 1)}$$

Then Green's theorem can be used to express the solution to (2.1) in terms of the boundary values of p_m and its normal derivative (e.g. Stakgold 1967),

$$p_m(r,x)=\int_{\partial\Omega}\left[\frac{\partial G_m^{(0)}}{\partial n}(r,x|r',x')p_m(r',x')-G_m^{(0)}(r,x|r',x')\frac{\partial p_m}{\partial n}(r',x')\right]\mathrm{d}S(r',x'), \quad (A\,2)$$

where $\partial\Omega$ is the boundary of Ω_0, and $\partial/\partial n$ represents the outward normal derivative with respect to the source coordinates (r',x'). Now, suppose that $G_m^{(0)}$ is subject to the conditions

$$\frac{\partial G_m^{(0)}}{\partial r}(r_0,x|r',x')=0, \quad x\in[0,L], \quad (A\,3a)$$

$$\frac{\partial G_m^{(0)}}{\partial x}(r,0|r',x')=\frac{\partial G_m^{(0)}}{\partial x}(r,L|r',x')=0, \quad r\in[r_0,r_1], \quad (A\,3b)$$

$$\frac{\partial G_m^{(0)}}{\partial r}(r_1,x|r',x')=-\eta_1\frac{\bar\rho_h}{\bar\rho_c}G_m^{(0)}(r_1,x|r',x'), \quad x\in[0,L], \quad (A\,3c)$$

for all $(r',x')\in\Omega_0$. Then, by substitution of these conditions and those on p_m into (A 2), we arrive at

$$p_m(r,x)=\int_{r_0}^{r_1}r'G_m^{(0)}(r,x|r',0)\frac{\partial p_m}{\partial x}(r',0)\,\mathrm{d}r'-\int_{r_0}^{r_1}r'G_m^{(0)}(r,x|r',L)\frac{\partial p_m}{\partial x}(r',L)\,\mathrm{d}r'$$
$$-\eta_1 r_1\frac{\bar\rho_h}{\bar\rho_c}\int_0^L G_m^{(0)}(r,x|r_1,x')p_m(r_1^+,x')\,\mathrm{d}x', \quad (A\,4)$$

for $(r,x)\in\Omega_0$. By imposing the vanishing normal derivative of the Green's function at $x=0$ and $x=L$, we have removed surface integrals involving the pressure on these boundaries. The compliance relation on the pressure at r_1 has introduced an integral involving p_m just outside the boundary, thus coupling the pressures in Ω_0 and Ω_1. Let us formulate a similar integral expression for p_m in Ω_k, $k\geqslant 1$, through the use of a Green's function $G_m^{(k)}$ which obeys

$$\frac{1}{r}\frac{\partial}{\partial r}\left(r\frac{\partial G_m^{(k)}}{\partial r}\right)+\frac{\partial^2 G_m^{(k)}}{\partial x^2}+\left(k_c^2-\frac{m^2}{r^2}\right)G_m^{(k)}=\frac{1}{r'}\delta(r-r')\delta(x-x') \quad (A\,5)$$

in Ω_k, as well as the conditions

$$\frac{\partial G_m^{(k)}}{\partial r}(r_k,x|r',x')=\eta_k G_m^{(k)}(r_k,x|r',x'), \quad x\in[0,L], \quad (A\,6a)$$

$$\frac{\partial G_m^{(k)}}{\partial x}(r,0|r',x')=\frac{\partial G_m^{(k)}}{\partial x}(r,L|r',x')=0, \quad r\in[r_{k-1},r_k], \quad (A\,6b)$$

$$\frac{\partial G_m^{(k)}}{\partial r}(r_{k+1},x|r',x')=-\eta_{k+1}G_m^{(k)}(r_{k+1},x|r',x'), \quad x\in[0,L]. \quad (A\,6c)$$

Then, simplifying Green's theorem through the application of boundary conditions as before, we find that

$$p_m(r,x)=-\eta_k r_k\int_0^L G_m^{(k)}(r,x|r_k,x')p_m(r_k^-,x')\,\mathrm{d}x'$$
$$-\eta_{k+1}r_{k+1}\int_0^L G_m^{(k)}(r,x|r_{k+1},x')p_m(r_{k+1}^+,x')\,\mathrm{d}x', \quad (A\,7)$$

for $k \geqslant 1$. The last integral couples the pressures in Ω_{k-1}, Ω_k and Ω_{k+1}. The procedure of developing integral expressions can be repeated until a rigid wall or plenum is reached, at either of which the series is truncated by virtue of a rigid-wall condition or negligible pressure fluctuations, respectively.

A.2. *Green's function development*

The boundary conditions at $x = 0$ and $x = L$ suggest a cosine expansion of $G_m^{(k)}$, provided that the series are uniformly convergent, which is verified in § 2.2. Assume the form

$$G_m^{(k)} = \frac{1}{L} \sum_{n=-\infty}^{\infty} R_n^{(k)}(r, r') \cos\left(\frac{n\pi x}{L}\right) \cos\left(\frac{n\pi x'}{L}\right), \tag{A 8}$$

for all regions k, where we have omitted the dependence of $R_n^{(k)}$ on the circumferential wavenumber, m. It can be shown that the solution for $k = 0$ is

$$R_n^{(0)}(r, r') = \frac{D_{n,<}^{(0)}(\tilde{\gamma}_n r_0, \tilde{\gamma}_n r_<) D_{n,>}^{(0)}(\tilde{\gamma}_n r_1, \tilde{\gamma}_n r_>)}{B_n^{(0)}}, \tag{A 9}$$

where $r_< = \min(r, r')$ and $r_> = \max(r, r')$. The inner, outer and combined functions are, respectively,

$$D_{n,<}^{(0)}(a, b) = Y_m'(a) J_m(b) - J_m'(a) Y_m(b), \tag{A 10a}$$

$$D_{n,>}^{(0)}(a, b) = \left[Y_m'(a) + \frac{\eta_1}{\tilde{\gamma}_n} \frac{\bar{\rho}_h}{\bar{\rho}_c} Y_m(a)\right] J_m(b) - \left[J_m'(a) + \frac{\eta_1}{\tilde{\gamma}_n} \frac{\bar{\rho}_h}{\bar{\rho}_c} J_m(a)\right] Y_m(b), \tag{A 10b}$$

$$\begin{aligned} \tfrac{1}{2}\pi B_n^{(0)} = &\left[Y_m'(\tilde{\gamma}_n r_1) + \frac{\eta_1}{\tilde{\gamma}_n} \frac{\bar{\rho}_h}{\bar{\rho}_c} Y_m(\tilde{\gamma}_n r_1)\right] J_m'(\tilde{\gamma}_n r_0) \\ &- \left[J_m'(\tilde{\gamma}_n r_1) + \frac{\eta_1}{\tilde{\gamma}_n} \frac{\bar{\rho}_h}{\bar{\rho}_c} J_m(\tilde{\gamma}_n r_1)\right] Y_m'(\tilde{\gamma}_n r_0), \end{aligned} \tag{A 10c}$$

for an annular duct, and for a cylindrical duct are given by

$$D_{n,<}^{(0)}(a, b) = J_m(b), \tag{A 11a}$$

$$D_{n,>}^{(0)}(a, b) = \left[Y_m'(a) + \frac{\eta_1}{\tilde{\gamma}_n} \frac{\bar{\rho}_h}{\bar{\rho}_c} Y_m(a)\right] J_m(b) - \left[J_m'(a) + \frac{\eta_1}{\tilde{\gamma}_n} \frac{\bar{\rho}_h}{\bar{\rho}_c} J_m(a)\right] Y_m(b), \tag{A 11b}$$

$$\tfrac{1}{2}\pi B_n^{(0)} = -J_m'(\tilde{\gamma}_n r_1) - \frac{\eta_1}{\tilde{\gamma}_n} \frac{\bar{\rho}_h}{\bar{\rho}_c} J_m(\tilde{\gamma}_n r_1). \tag{A 11c}$$

The radial wavenumber is defined as

$$\tilde{\gamma}_n = \begin{cases} \left|k_h^2 - n^2\pi^2/L^2\right|^{1/2}, & k_h L > n\pi, \\ \mathrm{i}\left|n^2\pi^2/L^2 - k_h^2\right|^{1/2}, & k_h L < n\pi. \end{cases} \tag{A 12}$$

Note that the branch chosen is not important, as the functions in which $\tilde{\gamma}_n$ appears are generally even with respect to it.

Similarly, the radial eigenfunction $R_n^{(k)}$ in region Ω_k, for $k \geqslant 1$, can be expressed as

$$R_n^{(k)}(r, r') = \frac{D_{n,<}^{(k)}(\bar{\gamma}_n r_k, \bar{\gamma}_n r_<) D_{n,>}^{(k)}(\bar{\gamma}_n r_{k+1}, \bar{\gamma}_n r_>)}{B_n^{(k)}}, \tag{A 13}$$

where

$$D^{(k)}_{n,<}(a,b) = \left[Y'_m(a) - \frac{\eta_k}{\bar{\gamma}_n} Y_m(a)\right] J_m(b) - \left[J'_m(a) - \frac{\eta_k}{\bar{\gamma}_n} J_m(a)\right] Y_m(b), \tag{A 14a}$$

$$D^{(k)}_{n,>}(a,b) = \left[Y'_m(a) + \frac{\eta_{k+1}}{\bar{\gamma}_n} Y_m(a)\right] J_m(b) - \left[J'_m(a) + \frac{\eta_{k+1}}{\bar{\gamma}_n} J_m(a)\right] Y_m(b), \tag{A 14b}$$

$$\begin{aligned} \tfrac{1}{2}\pi B^{(k)}_n = &\left[Y'_m(\bar{\gamma}_n r_{k+1}) + \frac{\eta_{k+1}}{\bar{\gamma}_n} Y_m(\bar{\gamma}_n r_{k+1})\right]\left[J'_m(\bar{\gamma}_n r_k) - \frac{\eta_k}{\bar{\gamma}_n} J_m(\bar{\gamma}_n r_k)\right] \\ &- \left[J'_m(\bar{\gamma}_n r_{k+1}) + \frac{\eta_{k+1}}{\bar{\gamma}_n} J_m(\bar{\gamma}_n r_{k+1})\right]\left[Y'_m(\bar{\gamma}_n r_k) - \frac{\eta_k}{\bar{\gamma}_n} Y_m(\bar{\gamma}_n r_k)\right], \end{aligned} \tag{A 14c}$$

and

$$\bar{\gamma}_n = \begin{cases} \left|k_c^2 - n^2\pi^2/L^2\right|^{1/2}, & k_c L > n\pi, \\ \mathrm{i}\left|n^2\pi^2/L^2 - k_c^2\right|^{1/2}, & k_c L < n\pi. \end{cases} \tag{A 15}$$

Again, the choice of branch is not crucial.

A.3. *Decoupling procedure*

The cosine expansion of the Green's function reduces each of the liner surface integrals in (A 4) and (A 7) to a projection of the liner pressure onto the cosine space. Define the projection coefficients as

$$\hat{p}^{\pm}_{k,n} \equiv \frac{1}{L}\int_0^L p_m(r_k^{\pm}, x)\cos\left(\frac{n\pi x}{L}\right)\mathrm{d}x. \tag{A 16}$$

Then, (A 4) can be written as

$$\begin{aligned} p_m(r,x) = &\int_{r_0}^{r_1} r' G^{(0)}_m(r,x|r',0)\frac{\partial p_m}{\partial x}(r',0)\,\mathrm{d}r' - \int_{r_0}^{r_1} r' G^{(0)}_m(r,x|r',L)\frac{\partial p_m}{\partial x}(r',L)\,\mathrm{d}r' \\ &- \eta_1 r_1 \frac{\bar{\rho}_h}{\bar{\rho}_c}\sum_{n=-\infty}^{\infty} R^{(0)}_n(r,r_1)\hat{p}^{+}_{1,n}\cos\left(\frac{n\pi x}{L}\right), \end{aligned} \tag{A 17}$$

and (A 7) as

$$\begin{aligned} p_m(r,x) = &-\eta_k r_k \sum_{n=-\infty}^{\infty} R^{(k)}_n(r,r_k)\hat{p}^{-}_{k,n}\cos\left(\frac{n\pi x}{L}\right) \\ &- \eta_{k+1} r_{k+1}\sum_{n=-\infty}^{\infty} R^{(k)}_n(r,r_{k+1})\hat{p}^{+}_{k+1,n}\cos\left(\frac{n\pi x}{L}\right). \end{aligned} \tag{A 18}$$

When (A 17) and (A 18) are evaluated on their bounding liner surfaces and projected onto the cosine space, the projection coefficients can easily be eliminated from the system of equations, and we can develop an integral equation for the pressure in Ω_0 that is uncoupled from the liner cavities.

When we carry out this projection on (A 17), evaluated at r_1, we find

$$\hat{p}^{-}_{1,n} = \hat{p}_{f,n} - \eta_1 r_1 \frac{\bar{\rho}_h}{\bar{\rho}_c} R^{(0)}_n(r_1,r_1)\hat{p}^{+}_{1,n}, \tag{A 19a}$$

where $\hat{p}_{f,n}$ represents the projection of the cross-section surface integrals in (A 17). Similarly, the projection of (A 18), evaluated at both r_k^+ and r_{k+1}^-, results in

$$\hat{p}_{k,n}^+ = -\eta_k r_k R_n^{(k)}(r_k, r_k)\hat{p}_{k,n}^- - \eta_{k+1} r_{k+1} R_n^{(k)}(r_k, r_{k+1})\hat{p}_{k+1,n}^+, \tag{A 19b}$$

$$\hat{p}_{k+1,n}^- = -\eta_k r_k R_n^{(k)}(r_{k+1}, r_k)\hat{p}_{k,n}^- - \eta_{k+1} r_{k+1} R_n^{(k)}(r_{k+1}, r_{k+1})\hat{p}_{k+1,n}^+. \tag{A 19c}$$

For a system consisting of N_l liners surrounded by a plenum (in which the outermost liner may be replaced by a rigid wall) there are $2N_l + 1$ coefficients and $2N_l + 1$ equations for each n. They can be solved to provide a generic relationship

$$\hat{p}_{1,n}^+ = Q_n \hat{p}_{f,n} \quad \text{(no sum over } n\text{)}. \tag{A 20}$$

where Q_n system-dependent. When this is substituted into (A 17), we finally arrive at the uncoupled integral equation,

$$p_m(r, x) = \int_{r_0}^{r_1} r' \tilde{G}_m(r, x|r', 0)\frac{\partial p_m}{\partial x}(r', 0)\,\mathrm{d}r' - \int_{r_0}^{r_1} r' \tilde{G}_m(r, x|r', L)\frac{\partial p_m}{\partial x}(r', L)\,\mathrm{d}r', \tag{A 21}$$

where the decoupling Green's function is given by

$$\tilde{G}_m(r, x|r', x') = \frac{1}{L}\sum_{n=-\infty}^{\infty} \tilde{R}_n(r, r')\cos\left(\frac{n\pi x}{L}\right)\cos\left(\frac{n\pi x'}{L}\right), \tag{A 22}$$

with

$$\tilde{R}_n(r, r') \equiv R_n^{(0)}(r, r') - \eta_1 r_1 Q_n \frac{\bar{\rho}_h}{\bar{\rho}_c} R_n^{(0)}(r, r_1) R_n^{(0)}(r_1, r'). \tag{A 23}$$

The radial function $R_n^{(0)}(r, r')$ is defined in (A 9).

A.4. *System factor* Λ_n

In § 2.2, integral equation (A 21) is developed into a solution scheme by introducing the boundary conditions for $\partial p_m/\partial x$ in terms of rigid-walled eigenfunctions, and performing the radial integration over r'. The resulting expression for the pressure $p_m(r, x)$ in (2.22), and ultimately for the system of algebraic equations (2.27a, b), contain modal coupling terms with a system-dependent factor Λ_n. This factor is defined as

$$\Lambda_n = \frac{2}{\pi}\frac{D_{n,<}^{(0)}(\tilde{\gamma}_n r_0, \tilde{\gamma}_n r_1)}{B_n^{(0)}}\left(1 + Q_n \frac{2}{\pi}\frac{D_{n,<}^{(0)'}(\tilde{\gamma}_n r_0, \tilde{\gamma}_n r_1)}{B_n^{(0)}}\right), \tag{A 24}$$

where the prime denotes differentiation with respect to the second argument. We provide here the form of Λ_n for three cases. It is easiest to first define a more compact notation. The duct and each cavity are represented in Λ_n by natural groupings of functions. Thus, we define

$$f_<^{(k)} \equiv \frac{2}{\pi}\frac{D_{n,<}^{(k)'}\left(\gamma_n^{(k)} r_k, \gamma_n^{(k)} r_{k+1}\right)}{B_n^{(k)}}, \quad C_<^k \equiv \frac{2}{\pi}\frac{\eta_{k+1}}{\gamma_n^{(k)}}\frac{D_{n,<}^{(k)}\left(\gamma_n^{(k)} r_k, \gamma_n^{(k)} r_k\right)}{B_n^{(k)}}, \tag{A 25a, b}$$

$$f_>^{(k)} \equiv \frac{2}{\pi}\frac{D_{n,>}^{(k)'}\left(\gamma_n^{(k)} r_{k+1}, \gamma_n^{(k)} r_k\right)}{B_n^{(k)}}, \quad C_>^k \equiv \frac{2}{\pi}\frac{\eta_k}{\gamma_n^{(k)}}\frac{D_{n,>}^{(k)}\left(\gamma_n^{(k)} r_{k+1}, \gamma_n^{(k)} r_{k+1}\right)}{B_n^{(k)}}, \tag{A 25c, d}$$

where the radial eigenvalue $\gamma_n^{(k)}$ takes the value appropriate to the region, either $\tilde{\gamma}_n$ or $\bar{\gamma}_n$.

First, for the case of a single liner and plenum, the system consists of only the duct and thus Λ_n is simply

$$\Lambda_n = f_<^{(0)}. \tag{A 26}$$

For a double liner and plenum (or single liner and rigid wall), the duct and adjacent cavity are both represented in Λ_n:

$$\Lambda_n = \frac{f_<^{(0)} f_>^{(1)}}{f_>^{(1)} - f_<^{(0)} + f_<^{(0)} f_>^{(1)}}. \tag{A 27}$$

Finally, for a triple liner and plenum (or double liner and rigid wall), the system term Λ_n contains the effects of the duct and both cavities:

$$\Lambda_n = \frac{f_<^{(0)}\left[\left(f_>^{(2)} - f_<^{(1)} + f_<^{(1)} f_>^{(2)}\right) f_>^{(1)} - C_<^{(1)} C_>^{(1)}\left(1 - f_>^{(2)}\right)\right]}{\left(f_>^{(2)} - f_<^{(1)} + f_<^{(1)} f_>^{(2)}\right)\left(f_>^{(1)} - f_<^{(0)} + f_<^{(0)} f_>^{(1)}\right) - C_<^{(1)} C_>^{(1)}\left(1 + f_<^{(0)}\right)\left(1 - f_>^{(2)}\right)}. \tag{A 28}$$

REFERENCES

Bechert, D. W. 1980 Sound absorption caused by vortex shedding, demonstrated with a jet flow. *J. Sound Vib.* **70**, 389–405.

Bellucci, V., Paschereit, C. O. & Flohr, P. 2002 Impedance of perforated screens with bias flow. *AIAA Paper* 2002-2437.

Crighton, D. G. 1981 Acoustics as a branch of fluid mechanics. *J. Fluid Mech.* **106**, 261–298.

Cummings, A. 1983 Acoustic nonlinearities and power losses at orifices. *AIAA J.* **22**, 786–792.

Cummings, A. & Eversman, W. 1983 High amplitude acoustic transmission through duct terminations: Theory. *J. Sound Vib.* **91**, 503–518.

Eldredge, J. D. & Dowling, A. P. 2003 The absorption of axial acoustic waves by a perforated liner with bias flow. *J. Fluid Mech.* **485**, 307–335.

Howe, M. S. 1979 On the theory of unsteady high Reynolds number flow through a circular aperture. *Proc. R. Soc. Lond.* A **366**, 205–223.

Howe, M. S. 1980 The dissipation of sound at an edge. *J. Sound Vib.* **70**, 407–411.

Hughes, I. J. & Dowling, A. P. 1990 The absorption of sound by perforated linings. *J. Fluid Mech.* **218**, 299–335.

Jing, X. & Sun, X. 1999 Experimental investigations of perforated liners with bias flow. *J. Acoust. Soc. Am.* **106**, 2436–2441.

Lansing, D. L. & Zorumski, W. E. 1973 Effects of wall admittance changes on duct transmission and radiation of sound. *J. Sound Vib.* **27**, 85–100.

Leppington, F. G. 1977 The effective compliance of perforated screens. *Mathematika* **24**, 199–215.

Levine, H. & Schwinger, J. 1948 On the radiation of sound from an unflanged circular pipe. *Phys. Rev.* **73**, 383–406.

Morse, P. M. & Ingard, K. U. 1968 *Theoretical Acoustics*. Princeton University Press.

Stakgold, I. 1967 *Boundary Value Problems of Mathematical Physics*. Macmillan.

Zhao, H. & Sun, X. 1999 Active control of wall acoustic impedance. *AIAA J.* **37**, 825–831.